Detection of mechanical waves in the left ventricle using high frame rate imaging

Kaja F. Kvåle

Series of dissertations submitted to the
Faculty of Mathematics and Natural Sciences, University of Oslo
No. 2318

ISSN 1501-7710

Cover: Hanne Baadsgaard Utigard.
Print production: Reprosentralen, University of Oslo.

Preface

This thesis is submitted to the Department of Informatics, Faculty of Mathematics and Natural Sciences, University of Oslo, as partial fulfillment of the requirements for the degree of Philosophiae Doctor. The research has been funded by the Center for Cardiological Innovation (CCI) – a research-based innovation center with funding from the Research Council of Norway and the consortium partners. The work was carried out under the supervision of Prof. Eigil Samset at GE Vingmed Ultrasound and the Department of Informatics, University of Oslo, and the co-supervision of Prof. Thor Edvardsen and MD Pål H. Brekke at the Center for Cardiological Innovation (CCI), and Sebastien Salles at the Department of Circulation and Imaging, Norwegian University of Science and Technology, between May 2016 and May 2020.

Acknowledgments

I want to thank the CCI and the Research Council of Norway for financing my research through the Ph.D. program, GE Vingmed Ultrasound for hosting me as an industrial Ph.D. student and the Department of Informatics at the University of Oslo for giving me the chance to pursue my Ph.D. It has been tremendously rewarding to be part of a multidisciplinary community and to experience the collaboration between industry and academia that I have had the opportunity to do during my research.

I would also like to thank my team of supervisors. A special thanks goes to my main supervisor Prof. Eigil Samset for your insight, helpful discussions, your thorough reviews of my work, and for pushing me forward. Additionally, I would like to thank my co-supervisors Prof. Thor Edvardsen, Pål H. Brekke and Sebastien Salles for your insight, discussions and guidance during my research. In particular, I would like to thank Pål H. Brekke for sharing your clinical expertise, your enthusiasm and for always keeping cold beverages in your office, and Sebastien Salles for sharing your technical expertise and for your continuous help throughout my whole Ph.D project.

I have been fortunate to have a large number of colleagues in a wide range of research groups. A special thanks goes to my former colleague at GE Vingmed Ultrasound, Jørn Bersvendsen, for your guidance in the early days of my project, my colleagues at the CCI, Espen W. Remme and John M. Aalen, for the collaboration on data collection and helpful discussions on theory and results, the ultrasound group at NTNU for providing me with data for my final article and for the fun times at conferences, and my fellow students at the University of Oslo for helpful discussions, coffee breaks and friendships.

Finally, I would like to thank my family and friends for the continuous encouragement, motivation, patience, love and support throughout these years.

Abstract

Cardiac ultrasound, or echocardiography, is an important part of modern cardiology and a key imaging modality to assess and quantify cardiac anatomy and function. In the past decade, high frame rate ultrasound imaging has emerged as a result of ultrasound image processing transitioning from being hardware based to software based. The increase in frame rate has allowed for studies of rapid phenomena that occur in the heart that were previously lost between frames with a conventional frame rate. However, the huge increase in frame rate also leads to a significant loss of spatial resolution that provides challenges in segmenting cardiac structures and interpreting the recorded information.

Many new applications have been investigated and proposed in literature with this new technology with the aim of using all this new information to aid with diagnosis and treatment planning for the cardiac patients. However, to make something useful out of the huge increase in information obtained, with frame rates up to several thousand frame per second, accurate and efficient methods for analysis are needed.

The aim for this thesis was to acquire ultrasound images at high frame rates and developing methods for analysis to detect and visualize phenomena that we have previously not been able to detect with ultrasound. The phenomena investigated here are the mechanical waves that propagate in cardiac tissue at high velocities. The main goal was to detect the properties of these waves to find useful characteristics to aid in non-invasive diagnosis of cardiac diseases that are currently diagnosed with invasive, time consuming and expensive methods.

Firstly, the regional mechanical activation of the heart was investigated for the purpose of detecting abnormal activation patterns which can be an indicator of conduction disorders. A method was developed to map and visualize the mechanical activation wave of the left ventricle (LV) from high frame rate ultrasound data, and its feasibility was demonstrated in an animal study. Data was acquired during pacing from several locations of the heart, and implanted electromyography (EMG) and sonomicrometry crystals were used as a reference standard. Our study showed that with our method we were able to approximately locate the origins of pacing and the propagation pattern of the mechanical activation wave. In addition, the results had a good agreement with the invasive reference standard.

Secondly, mechanical waves occurring naturally in the tissue after mechanical events in the heart were investigated for the purpose of using the propagation velocities to separate between healthy and pathological tissue. A method for velocity estimation was developed and its feasibility demonstrated in two studies using data from human populations. One study comparing mechanical wave velocities of healthy controls to a group of patients with myocardial infarcts was performed in order to detect locations of fibrosis. Regions of elevated velocities in patients were correlated with locations of myocardial infarcts found with late gadolinium enhanced magnetic resonance imaging (LGE-MRI). A sensitivity of 60% was found between the methods, with some regional differences in the LV. Another study assessing the velocities of several mechanical waves in healthy persons was performed for the purpose of increasing knowledge and information on the range of normal mechanical wave velocities.

For all studies, a novel signal processing method for mechanical wave detection, called Clutter Filter Wave Imaging (CFWI), was applied and tested. The CFWI-method was used as a replacement for the more conventional Tissue Doppler Imaging (TDI) method used for blood and tissue velocity estimation.

The main contributions of this thesis are the developed methods for analysis that have been evaluated for several clinical scenarios and validated against invasive and non-invasive reference standards. The methods have the potential of having clinical impact in the diagnosis of several cardiac pathologies related to conduction and tissue abnormalities.

Contents

Introduction

1.1 Background and motivation

Ischemic heart disease remains the world's most prevalent cause of death according to the World Health Organization [1], and cardiovascular disease accounts for 45 % of deaths in Europe [2]. Thus, there is a clear need for better and more accurate tools to assess cardiac anatomy and function, in order to perform proper diagnosis and treatment.

Medical imaging is a key component in the assessment of a patient's heart. Cardiac ultrasound, or echocardiography, has the benefit over other imaging modalities that it provides real time images of the beating heart, making it possible to assess anatomy and function at once. Additionally, echocardiography is inexpensive and less time consuming compared to other imaging modalities, it does not expose the patient to ionizing radiation, it is (generally) non-invasive, and the scanner can be brought to the patient's bed side.

A conventional ultrasound image is a grayscale two-dimensional (2D) image of a cross section of the patient's anatomy. Recent advancements in ultrasound technology have led to the possibility of three-dimensional (3D) volume imaging and to a significant increase in frame rate for 2D imaging from around 100 frames per second, to several thousand frames per second. While 3D imaging is used broadly in clinical practice, high frame rate imaging is still in the phase of investigation. With higher frame rate, a lot more information about short lived events in the cardiac cycle is available. It is possible to view the function of the heart in extreme slow motion and to capture events that would be lost between frames at a conventional frame rate. But with increased temporal resolution comes a reduction of spatial resolution. This happens because the only way to reduce the time spent per frame is to decrease the number of transmission beams used to create an image. This leads to reduced spatial resolution, which can only partly be recovered by intelligent signal progressing on the receive side. However, investigating what new and useful information can be extracted from high frame rate imaging has become a central new research field for echocardiography. Studies have shown improved tracking of blood flow, pulse wave propagation, cardiac contraction and brain activity because of high frame rate ultrasound imaging [3-5].

The focus of this thesis has been to test high frame rate imaging implemented in clinically available scanners, and to develop methods for analyzing the data to uncover rapid events in the heart that could possibly lead to clinical indicators of pathology or conduction disorders. Data have been acquired in several different settings, including an animal study involving implanted electrodes to pace the animals from several locations of the heart, and in patient studies with known myocardial infarcts and fibrosis that also underwent MRI. The rapid phenomena that have been studied for this thesis are the mechanical waves that propagate at high velocities in the myocardium following firstly, the electrical and mechanical activation of the heart, and secondly, mechanical events such as the closure of the valves. Our ultimate objectives have been,

1. to create an application for visualizing and quantifying electromechanical conduction, using a short ultrasound acquisition, which could ultimately replace contact electrophysiology (EP) mapping and dramatically reduce the time of cardiac procedures.
2. to visualize and quantify abnormal tissue characteristics, such as increased stiffness and abnormal conduction abilities, for the purpose of detecting ischemia, scar tissue and fibrosis using only a short ultrasound acquisition, ultimately replacing contrast magnetic resonance imaging (MRI).

For this thesis, the focus has been on the left ventricle (LV), as it is the main contributor to system pump function and responsible for pumping oxygenated blood to the brain, body and the heart itself.

1.2 Aims of study

The main goal of this thesis has been to investigate the use of high frame rate echocardiography acquired with a clinically available ultrasound scanner to uncover rapid events in the myocardium for the purpose of detecting pathology. More specifically we have investigated the pattern of electrical and mechanical activation of the LV, and the velocities of naturally occurring mechanical waves in the LV.

For optimal contraction and function of the heart, the contraction of the cardiac walls should be synchronous. The electricity, or depolarization wave, follows a specific pattern of propagation from cell to cell and along the fast tracks of the Purkinje network of the heart. The mechanical reaction following the depolarization, the mechanical activation wave, has been shown to follow the same pattern [6, 7]. For patients with ischemic heart disease, fibrosis or scar tissue, the propagation pattern of electricity in the myocardium may be altered causing suboptimal contraction and function, and cardiac arrhythmias. One of the treatment options for arrhythmias involves damaging tissue, to block electrical conduction, with a procedure called ablation. The success of the procedure depends on if the correct source of the arrhythmia was located. Thus, being able to detect and visualize locations of fibrosis and scar tissue in the myocardium would be beneficial for several reasons. Firstly, much time is spent locating the source causing arrhythmias in the ablation procedure and the procedure is invasive using a catheter. Hence, a non-invasive procedure would be a huge improvement for cost, time consumption and risk of complications for the patients. Secondly, a method to detect ischemic tissue, a reversible state for the myocardial tissue, would be hugely beneficial if it could contribute in preventing myocardial infarction and fibrosis and scars from forming.

It is the aim of the thesis to develop methods for detecting certain tissue characteristics to develop non-invasive tools that can aid in fibrosis, scar tissue, ischemia and arrhythmic source detection. To achieve this, high frame rate ultrasound data will be acquired to uncover rapid events that are undetectable with conventional imaging, and methods of analysis that make us able to take advantage of the increased amount of data will be developed.

In summary, this thesis aims to:

1. Investigate the clinical possibilities of high frame rate ultrasound imaging for pathology detection and develop methods for analysis of high frame rate ultrasound data.
2. Develop and test a method for detecting and visualizing regional mechanical activation in the left ventricle for the purpose of detecting arrhythmias.
3. Develop and test a method for estimation of propagation velocities of naturally occurring mechanical waves in the left ventricle for the purpose of myocardial fibrosis detection.
4. Test a novel signal processing method, Clutter Filter Wave Imaging, for mechanical wave detection.

1.3 Context of the project

This project has been funded by the Center for Cardiological Innovation (CCI), a research consortium of academic and industrial partners, sponsored by the Norwegian Research Council and hosted by Oslo University Hospital. The CCI has been a multi-disciplinary cooperation that brought together academic and industrial communities, including clinicians, mathematicians, computer scientists and industry, with the aim of developing the next generation of ultrasound systems for cardiology.

This project has been a cooperation between the CCI and consortium partners, and the University of Oslo. In such a project, there is a balance to be struck between academic and industrial endeavors. Therefore, obtaining clinically applicable solutions has been more central to this thesis than making theoretical contributions.

Background

This chapter aims to give the relevant background information necessary to understand the research done in this project. The main topics discussed are the human heart, ultrasound imaging, the difference between conventional and high frame rate imaging, details of tissue motion estimation, and detection of mechanical waves propagating through the myocardium. This presentation will be limited to information relevant for the papers contained in this thesis, as well as their discussion. However, references to helpful introductions and surveys are given throughout the text.

2.1 The human heart

2.1.1 Anatomy

The human heart consists of four cardiac chambers, two atria and two ventricles (see Fig. 2.1 for schematic drawing of the anatomy). The left side of the heart is responsible for receiving oxygen rich blood from the lungs and for supplying it to the body, brain and the heart muscle itself, and consists of the left atrium and the left ventricle (LV). The right side of the heart is responsible for receiving blood from the body and brain, and for pushing it to the lungs for oxygenation, and consists of the right atrium and right ventricle. Each side of the heart has two valves. Two of them sit between the atria and the ventricles (the A-V valves), and the other two between the ventricles and the outgoing arteries, the outflow valves. For the left side, the A-V valve is called the mitral valve and the outflow valve the aortic valve, and for the right side the A-V valve is called the tricuspid valve and the outflow valve the pulmonary valve. The valves open for filling of the cardiac chambers with blood, and close to prevent blood from going in the wrong direction. The motion of the valves is mostly passive and they open and close because of differences in pressure between the cardiac chambers and the arteries.

The heart is built up of four tissue layers. The endocardium, which is in direct contact with the blood inside the chambers. Then the myocardium, which consists of myocardial muscle fibers responsible for contraction. The epicardium is a membrane that envelopes the heart, and forms the innermost layer of the pericardium, which protects and separates the heart from surrounding tissue.

The muscle fibers in the myocardium are organized in muscle sheets swirling around the ventricles. When the fibers contract it results in a shortening in the long- and radial axes of the heart, and a torsion around the long axis, to squeeze out as much blood as possible from the ventricles. The result is that the heart works as a remarkably energy efficient, synchronous mechanical pump.

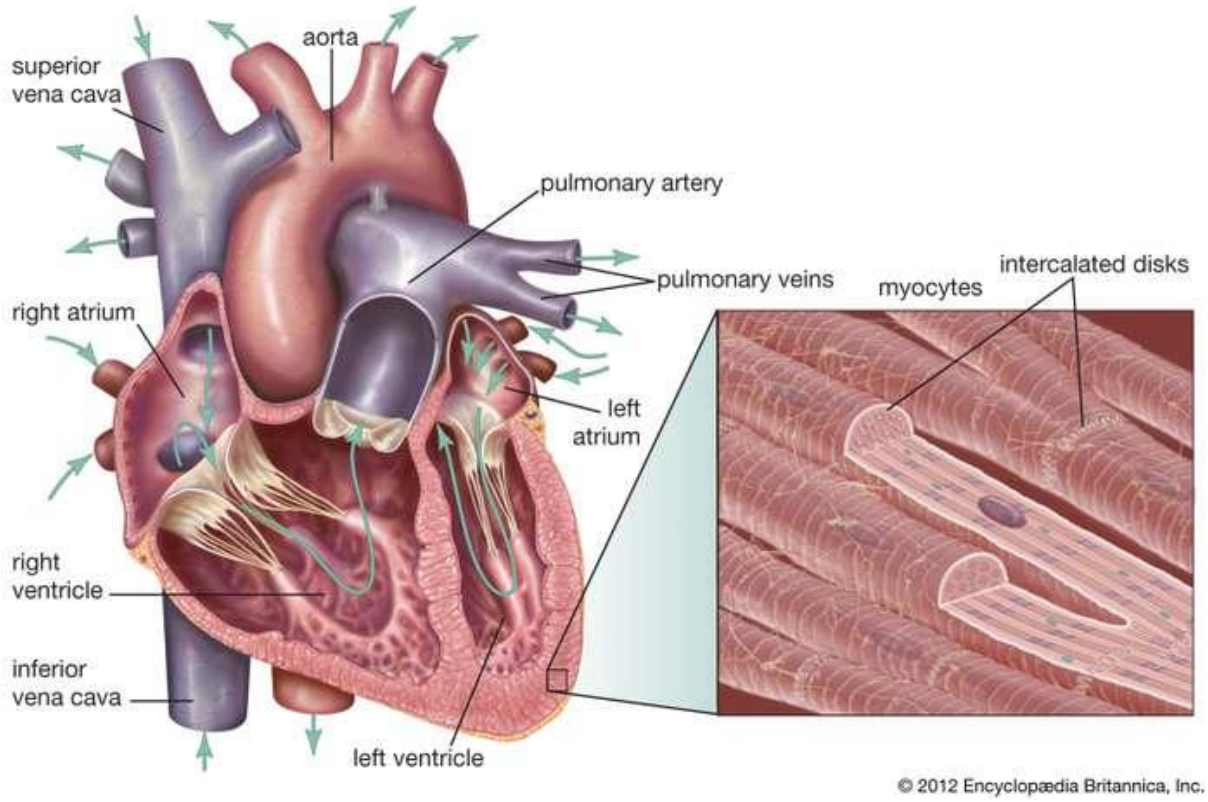

Fig. 2.1: Diagram of the heart anatomy. The green arrows indicate the direction of blood flow. On the right, the cardiac muscle cells are shown in detail in a zoomed illustration. Image reused from Encyclopædia Britannica.

2.1.2 Function

The cardiac cycle

Each cardiac cycle, or heartbeat, lasts for about one second (at rest, in humans) and consists of two main phases: the systole and the diastole. The ventricular diastole is the resting phase where the ventricles are relaxed and filled with blood from the atria. The A-V valves are open in this phase to allow for the filling of the ventricles, while the outflow valves from the ventricles to the arteries are closed. At the end of the ventricular diastole, the atria contract in the atrial systole, actively pushing blood into the ventricles. This is referred to as the atrial kick.

The ventricular systole follows and is the active contraction phase for the ventricles where blood is pumped from the ventricles to the circulatory systems. At the same time, the atria enter diastole and are filled with blood from the body and the lungs. During this time, the A-V valves are closed to prevent blood from flowing back into the atria, while the outflow valves to the arteries are open. When the ventricles are emptied, the pressure falls causing the outflow valves to close and the ventricles to enter diastole. The A-V valves then open for the ventricles to fill with blood and to relax in preparation for the next contraction.

Electrical conduction system

The mechanical contraction of the heart is regulated and coordinated by the electrical conduction system (Fig. 2.2). The system initiates an electrical impulse that propagates through the heart in a specific pattern, leading to electrical activation of the myocardium followed by contraction. The electrical activity in the heart is most commonly measured by surface electrocardiography (ECG). Electrodes placed on the skin record changes in voltage over time. The ECG waveforms (Fig. 2.3)

contain information about the heart rate and rhythm and can be used to uncover abnormalities in the conduction system. The electrical conduction system can be broadly divided into the impulse generating, but slowly conducting, nodes, and the impulse propagating His-Purkinje system. The sinoatrial (SA) node is the heart's natural pacemaker and produces the electrical impulse (or action potential) that depolarizes the heart and sets the heart rate. It is located in the right atrium (Fig. 2.2). The atrioventricular (AV) node also has inherent pacemaker activity but is suppressed by the higher rate of the SA node [8].

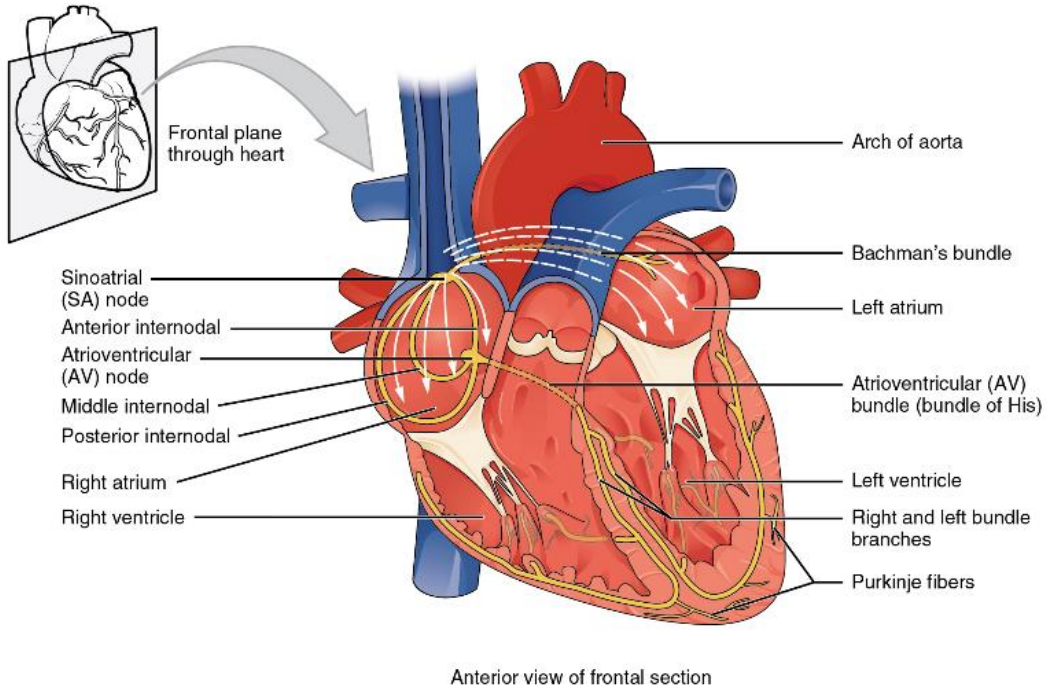

Fig. 2.2: The cardiac conduction system. Image from [9] published by OpenStax College, licensed under CC BY 4.0.

The pattern of propagation of the electrical impulse is shown in Fig. 2.3. From the SA node (step 2), the impulse spreads to the right atrium, followed by the left atrium directly from the right atrial muscle. The P-wave of the ECG is generated by the activation of the muscle of both atria. It also spreads rapidly through the right atrium to the AV node. Here, the impulse travels very slowly through the AV node delaying the signal slightly (step 3). This gives the atria time to contract in order to squeeze blood into the ventricles. After the AV node, which is the only pathway between the atria and the ventricles, the electrical signal is conducted very rapidly through the bundle of His, then through the bundle branches and to the respective Purkinje fibers for each side of the heart, and finally to the ventricular muscle (step 4). The interventricular septum is the first area of the ventricles to be electrically activated, generating the Q-wave of the ECG. Next, the ventricular free walls are activated, leading to the R-wave. Then, some late activated segments of the ventricles lead to the S-wave, and the depolarization of the ventricles is complete (step 5). Ventricular repolarization generates the T-wave (step 6), and begins at the apex, then spreads to the rest of the ventricles (step 1).

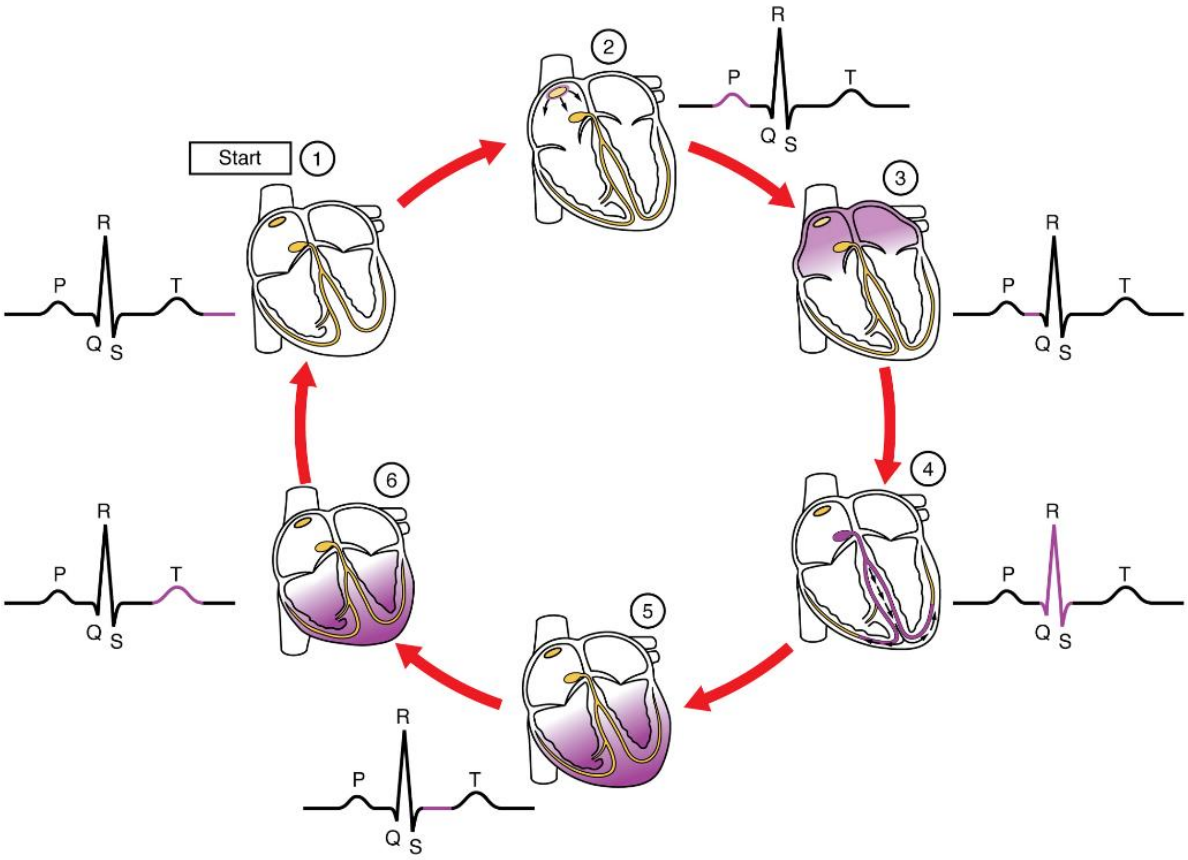

Fig. 2.3: The propagation of the depolarization wave. Images from [9]published by Openstax College, licensed under CC BY 4.0.

Cardiac electro-mechanics

The link between electrical activation and mechanical contraction, called excitation-contraction coupling, is found on the cellular level. The heart muscle consists of tubular muscle cells called cardiac myocytes (Fig. 2.1, right). Myocytes are able to shorten and lengthen because they contain myofibrils – the contractile unit of the cells. The myocytes have a negative resting membrane potential, meaning a negative internal charge. Once an electrical stimulus (flow of positively charged ions) reaches a myocyte, ion channels open in the cell membrane causing an inward flow of positive charge, and thus, depolarizing the cell. This leads to other cellular events that result in the conversion of the electrical energy of the action potential to shortening of the myofibrils (mechanical energy). The pacemaker cells that make up the nodes of the electrical conduction system are specialized myocytes. While the general myocytes have a large, stable resting potential and prolonged action potential, the pacemaker cells have a smaller, unstable resting potential which makes them depolarize spontaneously, and thereby generate the intrinsic electrical activity of the heart. Because gap junctions exist between myocytes, current flows rapidly between cells, allowing for a coordinated shortening of myofibrils. Furthermore, the myocytes are connected by *intercalated disks* (specialized adhesive junctions, Fig. 2.1) ensuring transmission of force from one cell to another leading to contraction of the muscle.

The activation of the heart is very complex as the electrical impulse travels rapidly along the cardiac conduction system, and simultaneously, slowly (in comparison) from myocyte to myocyte. In the ventricles, the Purkinje system is coupled to the myocardium at discrete sites (Purkinje-myocyte junctions). This means that cell-to-cell activation spreads from many locations at once, ensuring the coordinated activation of the ventricles. The conduction speed of the Purkinje network is much higher than that of cell-to-cell activation (1-4 m/s vs 0.3-0.5 m/s, respectively) [8, 10]. This is partially due to a type of gap junctions between these cells that allow for high conductance, and the high concentration

of them in the cell membranes [10]. Additionally, the Purkinje cells contain fewer myofibrils and are larger than regular myocytes.

The time lag from local depolarization to local onset of myocardial shortening is called the electromechanical delay (EMD). The EMD varies for different regions of the heart from a few milliseconds to as much as tens of milliseconds [11]. During sinus rhythm, EMD is greater at the epicardium than the endocardium, and greater at the base than near the apex. Late activated segments are characterized by a significant myofiber pre-stretch caused by contraction of early activated segments. This pre-stretch delays the onset of shortening in the late activated segments and results in a longer EMD [12]. However, active force generation by these segments is not necessarily delayed and can occur during pre-stretch. The regional mechanical activation can be defined as both the onset of shortening, and as the onset of active force generation. Active force generation is not load dependent, therefore, it is likely to better reflect timing of electrical activation [13]. Detailed knowledge of all three parameters are important to correctly identify the underlying mechanisms for a patient with a dyssynchronously contracting heart. Identifying if the problem is mainly electrical, mechanical or a combination of both is important for treatment planning [13].

2.1.3 Clinical indicators

Electrophysiology

Pathologies such as ischemia, inflammation, fibrosis, cardiomyopathies, or myocardial infarctions are likely to cause electrical and mechanical impairments in the heart. A myocardial infarction occurs when blood flow stops or decreases to a part of the heart causing damage to the heart muscle. Tissue cells that are cut off from a blood supply will die and eventually be replaced by scar tissue as a result of replacement fibrosis. This is to preserve ventricular integrity, facilitate force transmission and prevent rupture of the cardiac wall. However, the scar is not contractile and does not conduct electrical signals. Therefore, when a depolarizing impulse encounters a scarred area, it will move in alternative pathways around or slowly through the scar, leading to a delay in the impulse. If the delay is large enough for the myocytes to have repolarized, the delayed wave front can cause reactivation of tissue before a new signal is sent from the SA node. With the right timing, the reactivation signal can be caught in a re-entry loop that generates electrical impulses at a rate that suppresses the impulses from the SA node, and thereby cause an arrhythmia (abnormal and/or irregular heart rate). The described type of reentrant arrhythmia is just one of many types. Abnormally functioning tissue at any location in the heart can be a source of electrical impulses causing extra systoles that can lead to continuous arrhythmias. Some arrhythmias are harmless, while others can be life threatening.

Arrhythmias can be treated medically or with a procedure called ablation. Ablation consists of creating a block in the pathway causing the arrhythmia by damaging tissue using energy (heat or extreme cold) delivered through a catheter. An important success factor is that complete isolation of sources of abnormal electrical activity is achieved. For this, electrophysiological (EP) mapping is used where the local timing and voltage of electrical impulses is mapped with electrodes inserted through blood vessels. The information is used to generate maps of local voltage and/or timing of depolarization to identify sources of arrhythmias or areas of low voltage such as scar tissue (Fig. 2.4). This is a time consuming and invasive procedure as the generation of the map requires measurement of many spatial points. Thus, quick and non-invasive methods for activation mapping are needed, as abnormal activation patterns could be a clinical indicator of scar tissue, fibrosis and arrhythmias [14, 15].

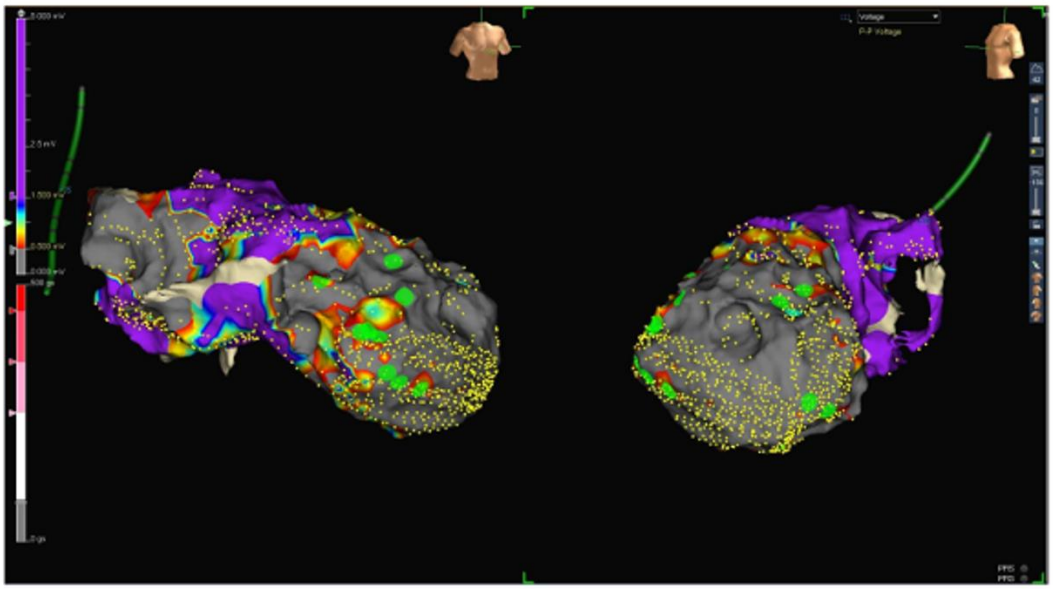

Fig. 2.4: An electroanatomical voltage map ranging from 0.5 to 1.5 mV generated from EP mapping using the EnSite system. A projection of the right atrium is shown on the left and the left atrium on the right. Small yellow dots represent the electro-anatomical mapping points. The voltage of ventricular signals is defined as scar below 0.5 mV (grey), the low voltage between 0.5 and 1.5 mV (from red to blue) and the normal voltage above 1.5 mV (purple, see the scale on the left side of the figure). Large green dots represent late potentials. Image from A. Schratter et al. [16] published by the Journal of Visualized Experiments (JoVe).

Myocardial ischemia

The most important cause of myocardial ischemia is reduction of blood flow through one or more coronary artery because of a partial or complete block of the artery. Ischemia can develop slowly over time from an artery that is gradually stenotic (coronary atherosclerosis), or quickly because of a sudden block such as a blood clot. Ischemia changes the metabolism of the heart cells. Normally, glucose and lipids are metabolized by oxidative reactions, but because of the inadequate supply of substrates (oxygen and glucose) to the cells, anaerobic metabolic processes become important. The change in metabolism, and the inadequate removal of products of metabolism (mainly protons and lactate), leads to intercellular events that impair contraction, and to a change in the net charge of the cell. The change in charge alters the duration of the action potential and the conduction of the cell, and can therefore cause arrhythmias [17]. Abnormal conduction patterns can therefore be a clinical indicator of ischemia. Prolonged and severe ischemia leads to myocyte death and tissue infarct.

Myocardial fibrosis

Myocardial fibrosis arises in the course of many heart diseases. Fibroblasts are cells that are located among the myocytes and that produce the connective tissue that forms the structural framework of the myocardium. When cardiac damage and stress occur, various substances cause the fibroblasts to become activated and transdifferentiate into myofibroblasts. Myofibroblasts have an increased production of proteins that are deposited in the extracellular matrix. This increase in collagen between myocytes leads to an increased stiffness of the myocardium [18, 19], and causes structural and electrical changes that predispose patients to arrhythmias, heart failure and ischemia. Increased myocardial stiffness is therefore a second clinical indicator of fibrosis.

Fibrosis is classified by cause and pathoanatomy. Replacement fibrosis, which was mentioned in the previous section, is local, caused by myocyte necrosis and thought to be irreversible. Interstitial (or

diffuse) fibrosis is characterized by diffuse spread of extracellular collagen and is believed to be reversible if treated early. This type is also seen in elderly people, and in diseases such aortic stenosis and coronary heart disease without infarction [19]. Fibrosis is currently diagnosed invasively with biomarkers measured in biopsies and blood tests, and non-invasively with MRI (with and without contrast), cardiac CT and echocardiography (by identifying areas of increased reflectivity).

2.1.4 Naturally occurring mechanical waves in the left ventricle

Several physiological processes, such as the vibrations induced by our vocal cords during speech, the mechanical contraction of the heart and the propagation of action potentials in our muscles, cause the body to constantly exhibit transient vibrations. These vibrations propagate through most organs and are mostly considered to spread as shear waves. The typical propagation velocity of shear waves in human organs ranges from 1 to 10 m/s, and the waves are therefore phenomena that last for milliseconds only. In addition, when pulsating blood moves through a large artery, transient mechanical stress is applied on the surrounding organs. This happens particularly in confined organs such as the brain or kidney.

In the heart, several events during the cardiac cycle induce transient movement in the tissue. Examples of these are the closure of the valves and the atrial kick. The resulting vibrations in tissue are called natural or intrinsic mechanical waves and propagate in the tissue at a certain velocity. Additionally, the propagation of the depolarization wave has been shown to generate a mechanical wave of the same pattern [6, 7]. This naturally occurring mechanical wave is not a shear wave, but rather a transient response of the tissue to the depolarization of the cells. The characteristics of the waves, such as the propagation velocities and patterns, give information about the medium they travel in, such as the stiffness or elasticity of the medium, and conduction paths for the activation wave, if detected and mapped. In an average size LV (with length of about 8 cm), the propagation of a shear wave in the longitudinal direction lasts for around 10 to 100 ms. Furthermore, the depolarization of the LV has a duration of less than 100 ms. Thus, to detect and map these waves a high sampling rate is required.

2.2 Echocardiography

Ultrasound are sound waves with frequencies above the audible range for the human ear (above 20 kHz). Medical ultrasound imaging uses sound waves in the frequency range from 1 MHz to 15 MHz, depending on the application. When applied to the heart, medical ultrasound is generally referred to as echocardiography, or simply *echo*. In this chapter, details of how an image is formed will be explained. Furthermore, an introduction of a method for tissue motion analysis from ultrasound data, Tissue Doppler Imaging (TDI), will be given, and the methods developed and applied for mechanical wave detection will be explained.

2.2.1 Image formation

For conventional ultrasound imaging, a line in an image is formed by transmitting ultrasound waves into an object in a specific direction, and recording the reflected signals, or echoes. In tissue, a reflecting object would be anatomical structures. The time from a signal is transmitted to an echo is recorded gives the distance to the object, and thereby the depth in the image. Furthermore, the intensity of the reflected echo is related to the density of the reflecting object.

The device responsible for transmission and reception of the ultrasound waves is called a transducer, or ultrasound probe, and is usually handheld on the patient’s skin. It consists of an array of piezoelectric elements that convert electrical pulses into sound pulses and vice versa. Pulses are

transmitted from each element at an ultrasonic frequency, resulting in an ultrasound beam. For the phased array transducer, the timing of transmission can be set individually for each element so that the beam can be focused and steered in different directions (Fig. 2.5a). The process of delaying the phase of transducer elements to steer the beam is called beamforming and is applied to both transmission and reception of ultrasound pulses. To create a full image using conventional imaging, the transducer scans across a region of interest, such as the heart, building the image line-by-line. The resulting two-dimensional image is called a brightness mode (B-mode) image because the different densities in the imaged medium are displayed on a gray scale (Fig. 2.5b). The dimensions of the image are called the axial and lateral directions, for the depth and width of the image, respectively. Another 2D image based on imaging the same line in space over time is called a motion mode (M-mode) image.

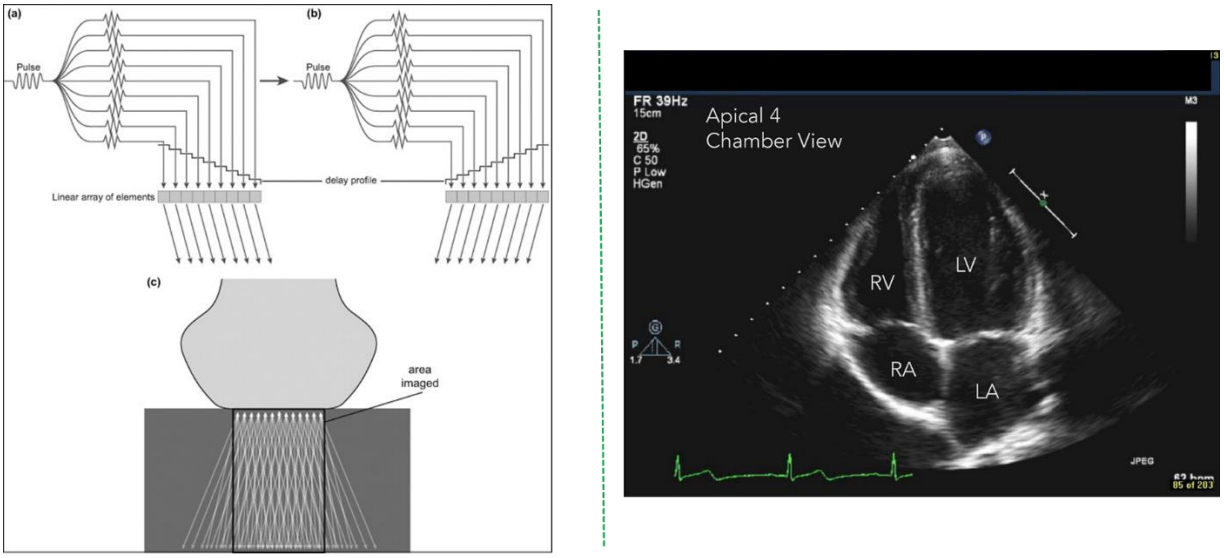

Fig. 2.5: (a) Illustration of a phased array with different delay profiles (a, b) that steers the beam in two different directions to cover an image sector (c). Image from A.J. Fischetti and A. Scott [20]. (b) An example of an ultrasound B-mode image of a human heart. The image is an apical 4 chamber view where RV is the right ventricle, LV the left ventricle, and RA and LA the right and left atrium, respectively. Image from [21] licensed under CC BY 4.0.

2.2.2 Transmission of ultrasound waves

Several types of waves can be transmitted by an ultrasound system. A focused wave is transmitted by delaying elements of the transducer so that the beam first has a wave front that converges towards a focus and then a diverging wave front. In the focus the beam is narrow, and the amplitudes are added for maximum intensity. A plane wave is generated by transmitting from all the elements of the transducer array without delay, resulting in a wide homogenous beam. A diverging wave is a defocused beam that spreads to a larger field of view with depth, creating a sector scan. Cardiac imaging uses a sector scan since the transducer must be placed in between the ribs, and therefore is restricted to a small *acoustical window*.

2.2.3 Resolution

Resolution is important for the image quality. For ultrasound imaging, there is spatial, contrast and temporal resolution. The ability of an ultrasound system to distinguish between two points in space is determined by spatial and contrast resolution, and the ability to distinguish between two events in time

is determined by the temporal resolution. The axial resolution is the minimum distance that can be differentiated between two reflectors located parallel to the direction of the ultrasound beam, and it is effectively half the received pulse length. The pulse length is a product of the number of cycles in the pulse and the wavelength. Axial resolution is high when the pulse length is short, which means that few cycles and short wavelength is equal to high resolution. The number of cycles is determined by the damping factor of the transducer elements after excitation, while the wavelength is determined by the transmit frequency. High damping and high frequency gives few cycles and short wavelength, which results in high axial resolution [22]. However, high damping leads to a low intensity pulse, and high frequency leads to high attenuation by tissue, especially in locations further from the transducer.

The lateral resolution is the minimum distance that can be differentiated between two reflectors at the same depth and is high when the width of the beam is narrow. For a focused beam this width varies with depth, being the narrowest at the focus depth, with a width equal to half the transducer width. The beam width is the product of the focus depth and the wavelength of the pulse, divided by the transducer (or aperture) width. Lateral resolution is therefore better for larger apertures and higher transmit frequencies.

Temporal resolution is a combination of the propagation velocity of sound waves in soft tissue, the imaging depth and the size of the image sector, meaning the number of transmitted beams. Thus, for a narrower and shallower image sector, a higher frame rate can be achieved because fewer beams must be transmitted and the system must wait a shorter amount of time before transmitting a new beam in the next direction. A high spatial resolution increases the image quality but requires denser sampling and more scan lines which reduces the frame rate.

Contrast resolution is the ability of the ultrasound system to distinguish between different echo amplitudes of adjacent structures. It is measured as the contrast-to-noise ratio (CNR) and affected by the *side-lobes* in the transmitted beam which causes the system to receive echoes from outside of the main beam.

2.2.4 Multiple line acquisition (MLA)

One of many solutions developed to increase temporal resolution is multiple-line acquisition (MLA). The concept of MLA is to acquire more than one receive line for each transmission which allows for fewer transmit events per image. The technique is also called parallel beamforming as the receive lines are created in parallel. The potential frame rate increase compared to conventional single line acquisition is equal to the number of parallel beams acquired. MLA significantly increases the data acquisition rate. This can be used to increase temporal resolution, to increase the signal-to-noise ratio (SNR) for a conventional frame rate (by averaging over several frames), to increase the field-of-view, or a combination of all.

MLA is used in combination with a wider transmit beam as a larger sector must be imaged per transmit. A wider beam corresponds to a smaller transmit aperture which gives a poorer lateral resolution compared to focused imaging. In addition, a small aperture results in higher side lobe levels which reduces the contrast resolution, and a wider, less-focused beam has a lower intensity which reduces penetration and gives a lower SNR in the lower parts of the image [5, 22]. Thus, for maximum image quality, it is beneficial to transmit beams that are as focused as possible.

2.2.5 Tissue Doppler Imaging

The Doppler Effect is a fundamental principle utilized for both tissue motion estimation and blood flow detection with ultrasound, and it describes the phenomenon where the observed frequency is different for a moving object and an observer at rest. As ultrasound is based on frequency modulated

wave transmission, the received frequency will be changed if the imaged object is in motion relative to the probe. The frequency shift can be used to detect the velocity of the moving object in the beam direction using the below equation

$$f_D = 2f_0 \frac{v}{c} \cos \alpha, \quad (1)$$

where f_D is the Doppler shifted frequency, f_0 the transmitted frequency, v the velocity of the moving object, c the speed of sound and α the angle between the ultrasound beam and the direction of motion.

In practice, the velocity analysis in the ultrasound scanner is done in terms of the phase shift between two or more returning pulses. The analysis is called autocorrelation estimation and is based on estimating the delay in phase between similar signals with a certain temporal lag. If two ultrasound pulses are shot successively in the same direction towards a moving object, the returning signals will remain fairly constant, however, the phases will have shifted from one another as the imaged object has moved slightly towards or away from the transducer. This phase delay from one signal to another can be utilized to estimate the velocity of the moving object [23, 24], using the below equation

$$\hat{V} = \frac{\angle \hat{R}_x(1) \times vNyq}{\pi}, \quad (2)$$

with

$$vNyq = \frac{c_0 \times FPS}{4 f_0}, \quad (3)$$

where $\angle \hat{R}_x(1)$ represents the phase angle of the estimates from the autocorrelation of ultrasound signals with a temporal lag of one, c_0 the speed of sound, FPS the frame rate and f_0 the transmit frequency of the transducer.

Tissue motion estimation is an important feature in echocardiography. Today, Doppler based tools are mandatory on every medical ultrasound device, especially within the framework of cardiovascular and cancer diagnostic applications.

2.3 High frame rate ultrasound imaging

Conventional, or focused, echocardiography normally has a frame rate of 50 to 100 frames per second. This is equal to an image being acquired every 10 to 20 ms and is sufficient for most standard applications and measurements. However, to study rapid physiological phenomena occurring in the human body, such as the naturally occurring mechanical waves previously described, a higher frame rate is required [5, 23]. For the projects that this thesis is comprised of, a frame rate of at least 1000 (and up to 1800) frames per second has been used. This temporal resolution results in a minimum of about 100 frames acquired during the period of propagation for a wave of interest, which gives the opportunity to detect the wave front in detail.

High frame rate ultrasound imaging has become possible over the last 10 to 20 years due to a shift from hardware to software based technologies in the ultrasound scanner, and because of the availability of fully programmable research ultrasound systems [25]. Received echoes were previously processed using specialized hardware which limited the number of MLAs created in parallel. However, as computational power in personal computers has increased, much of the signal processing, including the beamforming, has been moved to programmable graphics processing units (GPUs). This move from hardware to software beamforming has allowed for the possibility to create an unlimited number of MLAs in parallel, which has brought us to the extreme case of creating a full image from one

transmission only. To cover an entire image sector with one transmission, plane wave or diverging wave imaging can be used. These approaches suffer from poor image quality in terms of spatial resolution and contrast because of the small apertures, width of the beams and low pressure applied by these waves compared to a focused wave, as previously mentioned. Fig. 2.6 visualizes the trade-off between frame rate and image quality represented by spatial resolution and SNR. Image quality can be increased by compounding, but that will again decrease the temporal resolution. For this thesis, weakly focused beams were used with 4 to 6 transmissions per image. The blue circle in Fig. 2.6 illustrates where the method used for this thesis is located on the frame rate vs image quality trade-off scale.

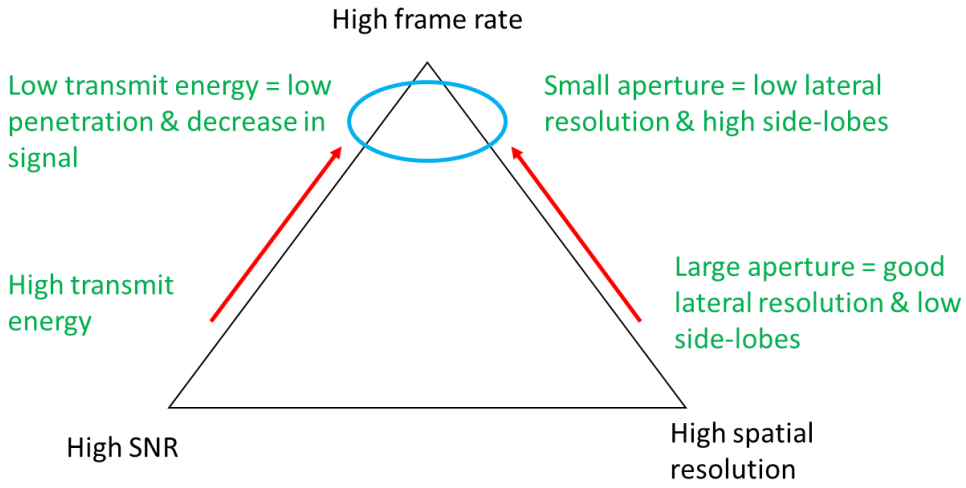

Fig. 2.6: shows the trade-off between SNR, spatial resolution and high frame rate imaging. The blue circle illustrates the edge cases of plane and diverging wave imaging, the weakly focused beams used for this thesis, and unlimited MLAs.

2.4 Mechanical wave estimation in the left ventricle with echo

This chapter will serve as an introduction to the field of mechanical wave imaging. Important historical developments and research will be mentioned, and the methods developed and used for this thesis will be introduced.

2.4.1 Mechanical waves

Artificially produced mechanical waves

The first clinical application for high frame rate, or ultrafast, ultrasound imaging was introduced in the field of elasticity imaging with the objective of tracking shear waves induced in tissue by a transient vibration from the surface of the body, in real time [26-28]. Shear waves are short-lived mechanical waves that propagate through an object whenever a pressure that causes the object to deform is applied. The propagation velocity of a shear wave traveling in homogenous and isotropic solids is equal to the square root of the ratio of the constant shear modulus (G) in Pa (i.e. stiffness) for the medium, to the density (ρ) in kg/m^3, of the medium,

$$v = \sqrt{\frac{G}{\rho}}. \qquad (4)$$

Thus, hard lesions, such as tumors, could be discovered in, and distinguished from, soft tissue using the relationship between shear wave speed and local elasticity of the medium, as shear waves should have a higher velocity in a hard medium than in a soft medium. This was shown in breast tissue by J. Bercoff *et al.* [28].

There are several ways to induce shear waves in tissue for shear wave imaging. One commonly used method is to attach an externally vibrating source to a transducer and place it on the surface of the body [26]. Another method is to use the acoustic radiation force impulse (ARFI) generated by the ultrasonic probe itself. Doherty *et al*. imaged the displacements induced by acoustic radiation force in the organ at an ultra-high frame rate, and from this were able to estimate the local shear wave speed, which allowed for the generation of a quantitative map of tissue stiffness [29]. Artificially produced mechanical waves have a high frequency content and can be induced at any time, which is beneficial. However, strong attenuation by the tissue makes this method more suitable for shallow depths, such as the breast and liver.

Naturally occurring mechanical waves in the LV

Naturally occurring waves in the heart resulting from numerous mechanical events were described in section 2.1.4. These waves have a lower frequency content than artificially produced waves and are therefore less attenuated by tissue and can propagate longer in organs. This is beneficial for studying deeper lying structures in organs such as the heart, especially for closed chest applications. However, a disadvantage is that they cannot be produced at any time as data acquisition needs to be timed with the cardiac cycle.

In the LV, several natural waves have been described. H. Kanai and colleagues have shown multiple mechanical waves propagating along the septum [30, 31]. In the late 1990s and the early 2000s, they were the first to image and track these waves in the field of cardiovascular ultrasound [30, 32, 33]. One goal of these studies was to capture the rapid motion, or vibrations, in LV tissue for the purpose of distinguishing myocardial fibrosis from healthy tissue. High frame rate imaging was not available at that time, but they were able to image the transient propagation of mechanical waves by repeating the experiment over several cardiac cycles using conventional imaging.

Mechanical activation wave

A natural wave occurring around the time of the Q-wave in the ECG was detected in the LV by H. Kanai and colleagues, and found to propagate from the middle of the interventricular septum towards the base and apical sides of the heart [30, 31]. The wave was recognized as the propagation of electrical activation from the Purkinje-myocyte junctions in the interventricular septum. This was also demonstrated by Provost *et al*. in an animal study in 2011, where they showed that the velocity of this wave was strongly correlated with the propagation of the depolarization wave [34]. From 2005, Pernot and Konofagou tracked the propagation of this wave (referred to by them as the electromechanical wave) in the myocardium of rodents [35-37]. The objective was not to estimate the velocity of the wave, but rather to capture the propagation pattern for the purpose of detecting abnormal electrical conduction in the LV. In 2012, Provost *et al*. performed the first clinical evaluation of electromechanical wave imaging (EWI) in patients [38] using a single heartbeat approach [39]. Later on, the same research group has used the EWI method to investigate ischemic hearts [40] and atrial [41] and ventricular [14] arrhythmias [7, 42, 43], as well as expanding the method to 3D [15].

Naturally occurring shear waves

Several waves that originate at the base of the interventricular septum and propagate towards the apex can be detected in the LV (see example in Fig. 2.12a). These have been identified as shear waves resulting from mechanical events that occur in the heart. One wave originating around the time of the atrial kick was shown to propagate with a velocity of 1 to 4 m/s [31, 44]. Another wave arose around

the time of the aortic valve closure (AVC) and propagated with the same velocity [45], and yet a third around the time of the mitral valve closure (MVC) propagating with a velocity of 1 to 7 m/s [30].

With the recent availability of high frame rate ultrasound imaging, the characteristics of these waves have been studied with a single heartbeat acquisition. Recently, Santos *et al*. investigated the waves occurring from mitral and aortic valve closure to establish the stability of the occurrence of the waves, the reproducibility of the wave detection and the normal range of the propagation velocities [46]. Additionally, healthy volunteers and patients were studied to find differences in propagation velocities that could be used as an indicator of pathology. Later, the same research group evaluated the relation between shear wave velocity and myocardial stiffness in patients and healthy volunteers [47].

2.4.2 Mechanical wave detection

There are several approaches to natural mechanical wave detection, but the methods have some steps in common. These are visualized in the flow chart in Fig. 2.7. The first step is to acquire high frame rate ultrasound images and extract signal data (in-phase and quadrature (IQ) data) from the ultrasound scanner. Then, tissue motion analysis is performed on the signals to estimate the velocity of the imaged tissue (step 2). For all projects of this thesis, the Clutter Filter Wave Imaging (CFWI) method was used (step 3b), and for one project (paper III), tissue velocity imaging (Electromechanical Wave Imaging (EWI) using TDI, section 2.2.5) was applied (step 3a). The two different approaches will be described in detail in the following sections. The next step consists of finding the derivative of the velocity data in space (strain rate, step 4a) and time ((CFWI) acceleration, step 4b). From this the arrival of the wave front of the mechanical wave can be mapped temporally for every imaged spatial point of interest. The definition of wave front for one spatial point differs for the two approaches: from zero-crossing of the strain rate curve (step 5a), to maximum/peak acceleration of the (CFWI) acceleration curve (step 5b). The propagation of the wave front in space and time was visualized in a spatiotemporal isochrone map (step 6) for three of the projects of this thesis (papers I, II and III).

The isochrone map can be used to find the propagation velocity of the mechanical wave (step 7). The propagation velocity was estimated for two of the projects of this thesis (papers II and IV), and for paper II the isochrone map approach was used. The details of the propagation pattern mapping and velocity estimation will be explained in the following sections.

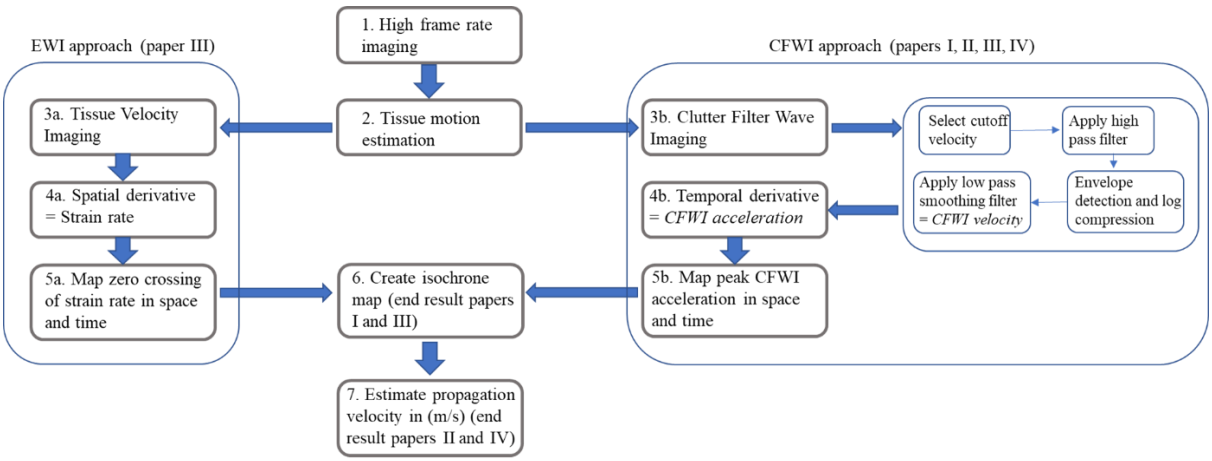

Fig. 2.7: Flow chart of the mechanical wave detection methods.

2.4.3 Clutter Filter Wave Imaging

Velocity estimation is an important feature in ultrasound imaging and is the basis of analyses that involve motion of either blood or tissue. TDI, described in section 2.2.5, is the most common technique for velocity estimation and is based on detecting the phase difference of a signal at a certain time lag. Other techniques include block matching and methods based on cross correlation of the signal [24, 48]. There are advantages and disadvantages to every approach, but mainly, TDI allows for sub-pixel estimation without interpolation, and is thus less computationally expensive. However, velocity is only estimated in the axial direction whereas block matching techniques can be two-dimensional.

For this thesis, tissue motion has been detected using CFWI. For blood flow velocity estimation, a clutter filter is normally used to fully remove low-frequency tissue motion to accentuate the high-frequency movement from blood. For several of the projects in this thesis, the clutter filter has been used for another purpose – to selectively attenuate, and thus accentuate, tissue motion of interest. The motion of interest will then be observable as darker intensity bands propagating in the B-mode images [49, 50]. While only the locality and not the velocity of motion is detected, it has been shown that this method is more sensitive to subtle tissue displacements compared to TDI [50].

Principle

The principle is shown in Fig. 2.8. The method consists of applying a carefully designed high pass filter to the ultrasound signal data. The stop and transition band of the filter is used to attenuate a desired band of tissue velocities. Thus, a priori knowledge of the velocities of interest is necessary. After filtering, the ultrasound B-mode images will display darker intensity bands propagating in tissue, as wave fronts of mechanical waves. The waves can then be tracked to find mechanical wave propagation patterns and velocities

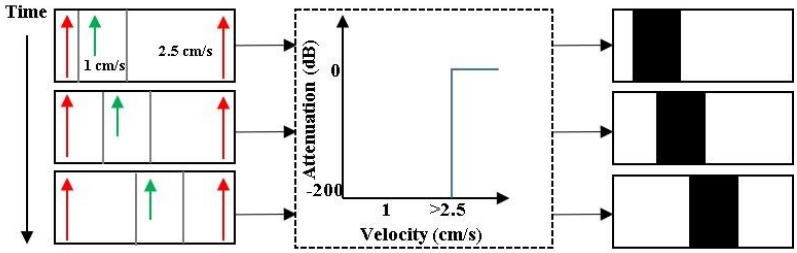

Fig. 2.8: The principle of CFWI. The figure shows a high pass filter with a cutoff velocity equal to 2.5 cm/s, thus, all tissue velocities below this cutoff will be attenuated. (Figure from paper I) @IEEE2019

Method

The steps of the method are shown in Fig. 2.7 (step 3b). The most important parameter of the clutter (high pass) filter is the cutoff frequency. The normalized cutoff frequency, fc_n, of the filter is defined as

$$fc_n = Vc \big/ vNyq, \tag{5}$$

with

$$vNyq = \frac{c_0 \times FPS}{4 f_0}, \tag{6}$$

and,

$$fc = {fc_n \times FPS}/{2}, \qquad (7)$$

where Vc is the cutoff velocity, c_0 is the speed of sound, FPS is the frame rate, f_0 the transmit frequency, v_{Nyq} the Nyquist velocity and f_c the cutoff frequency in Hz.

After applying the clutter filter on the ultrasound IQ data, the B-mode images are extracted by envelope detection and logarithmic compression of the filtered ultrasound signals. Spatiotemporal smoothing, in the form of a low pass filter, is then applied to increase the SNR. The output, a filtered B-mode sequence, gives an image of the tissue velocity similar to the result from using TDI velocity estimation. The filtered B-mode sequence has been referred to as (CFWI) velocity for the projects of this thesis. Furthermore, to obtain an image of tissue acceleration ((CFWI) acceleration), the filtered B-mode sequence is differentiated in time (Fig. 2.7, step 4b). Mechanical wave propagation pattern and velocity can then be determined from tracking the peaks/maxima of (CFWI) acceleration in space and time (Fig. 2.7 steps 5b-7 and 2.10b).

For the projects of this thesis, the cutoff velocity was found from estimating the approximate tissue velocities at different times of the cardiac cycle using TDI. The tissue velocities were then converted to normalized cutoff frequencies using Eq. 5. For the high pass clutter filter, a third order Butterworth filter was used in all estimations. The low pass smoothing filter used for all projects was a third order Butterworth filter with a cutoff frequency of about 30 Hz.

2.4.4 Mechanical wave propagation pattern detection

The propagation pattern of the mechanical activation wave was mapped for the first and third contributions of this thesis, and the propagation pattern of the mechanical shear wave following the atrial kick was mapped for the second contribution of this thesis to use for propagation velocity estimation. Fig. 2.9 (left) shows the propagation of the mechanical wave following the atrial kick in the LV at three different points in time represented by peak (CFWI) acceleration. In the middle, the detection of the wave front for one spatial point is shown, and the resulting isochrone map is shown on the right.

The first step of mapping the propagation of the wave front consists of selecting the time interval in the cardiac cycle for the wave of interest. Second, determine the time of peak acceleration for every spatial point within the time interval, and display the result in an isochrone map. The isochrone map gives an image of the mechanical wave propagation pattern where the color scale (in milliseconds) maps to time to peak acceleration. From this, the propagation velocity of a mechanical wave can be derived.

For the detection of the activation wave, the (CFWI) velocity was used to define the wave front. In the TDI velocity trace, a negative velocity feature is caused by atrial induced filling, followed by a positive pre-ejection spike caused by mitral valve closure. In between, the LV has been mechanically activated, therefore, the maximum/peak acceleration of the pre-ejection spike was used to define the time of mechanical activation. To ensure the correct acceleration peak (wave front) was selected, a certain threshold was set for the (CFWI) velocity trace to reach within the defined time interval before the automatic search for a (CFWI) acceleration peak began. As the activation wave follows both the Purkinje-network and cell-to cell activation, the propagation pattern is much more complex than that of a shear wave induced by a mechanical event.

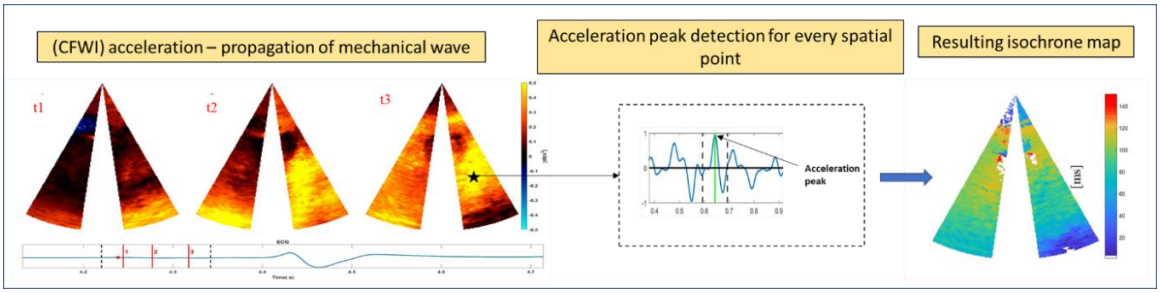

Fig. 2.9: The figure shows the propagation of the atrial kick wave through the LV at three different points in time (left). In the middle, peak acceleration detection is shown for one spatial point, then the resulting isochrone map of the propagation pattern on the right. The colormap of the isochrone map is in (ms). (The figure is partially reused from paper II).

2.4.5 Electromechanical activation wave imaging

For the project in paper III we aimed to compare the feasibility, accuracy, and time consumption of the CFWI method developed for mechanical activation wave detection [51] to EWI. EWI consists of spatiotemporally mapping the electromechanical wave, by mapping a transient response to the depolarization in the tissue. This translates to spatiotemporally mapping the time of zero-crossing in a strain rate trace (Fig. 2.10) for every spatial point of interest. As strain rate represents the rate of change in length of a segment (in the axial direction), the zero crossing represents a change from lengthening to onset shortening. However, strain rate is a second derivative and therefore susceptible to noise. Substantial filtering and smoothing is therefore required [23]. A version of this method was implemented where we used TDI for tissue motion analysis (as opposed to CC-methods used by the Konofagou group) mentioned in section 2.4.1. The steps of the method implemented for this thesis are outlined in Fig. 2.7 (steps 3a-6).

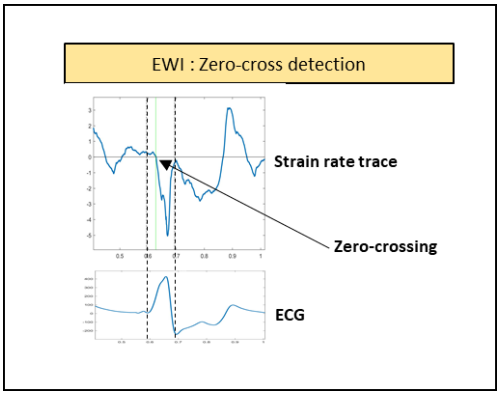

Fig. 2.10: Example of the zero-cross detection of the EWI method for one spatial point.

.

2.4.6 Mechanical shear wave velocity estimation

The velocities of several mechanical waves were estimated for the second and fourth contributions in this thesis. For the second project, the wave occurring around the time of the atrial kick was studied for the purpose of separating infarct patients from healthy volunteers by differences in propagation velocity. The same wave was studied in the fourth project, in addition to the mechanical waves occurring around the time of AVC and MVC, for a small group of healthy volunteers. For most studies in this area, spatiotemporal TDI acceleration maps (M-mode plots) have been used for mechanical wave velocity estimation. For this thesis, (CFWI) acceleration has been used for this purpose (Fig. 2.11-12).

In paper II, mechanical wave velocity was estimated from an isochrone map (Fig. 2.11). The method consisted of estimating velocity separately in the two spatial directions (x and y) by calculating gradients from the isochrone map. This step was repeated 5 times using different length segments resulting in 5 velocity matrices which were averaged to obtain one velocity matrix in each spatial direction (V_x and V_y). These were combined using the equation from Fig. 2.11, resulting in a map of the mechanical wave velocity in (m/s) for every imaged spatial point (Fig. 2.11, right).

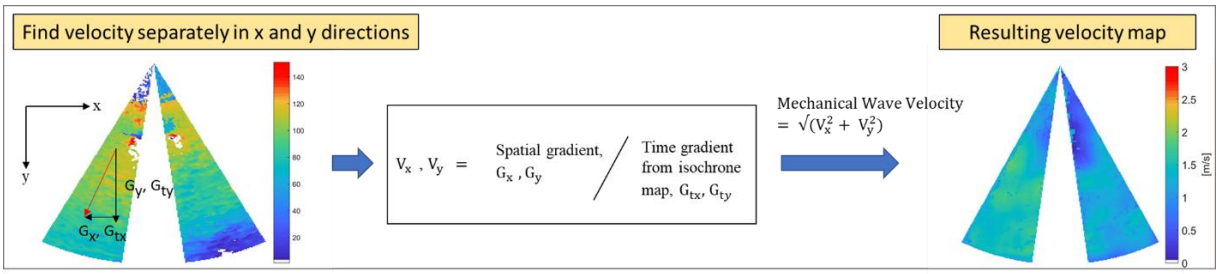

Fig. 2.11: The figure shows an isochrone map on the left with time and spatial gradients marked. In the middle, the velocity calculation using the gradients is shown, then the resulting velocity map (in m/s) is shown on the right. (The figure is partially reused from paper II).

For paper IV, only one mechanical wave velocity value per heart chamber wall was estimated. The CFWI processing was the same, but the mechanical wave velocity estimation method consisted of plotting the (CFWI) acceleration for the spatial coordinates of the mid heart wall over time (an anatomical M-mode plot), and then fitting a line to the maximum/peak acceleration (or wave front) using linear regression analysis. The mechanical wave velocity (in m/s) was then found from the slope of the line.

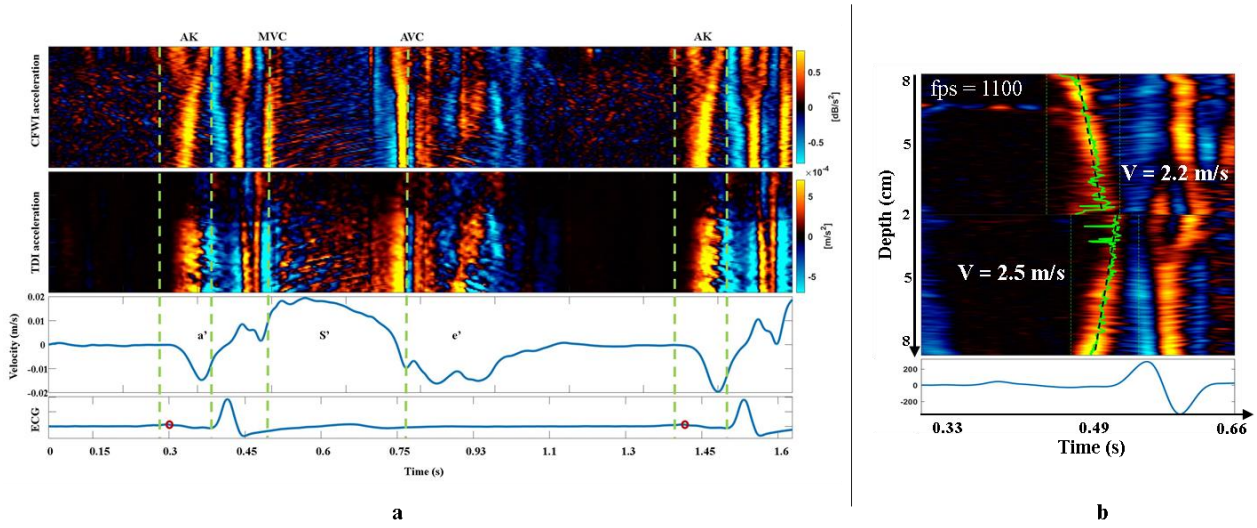

Fig. 2.12: (a) Naturally occurring mechanical waves in the LV represented by a (CFWI) acceleration M-mode image. AK is the atrial kick, MVC the mitral valve closure and AVC the aortic valve closure. A TDI velocity trace and ECG trace have been added for timing purposes. (Figure from paper II). (b) A zoomed in version of (a) for two heart walls. An example of mechanical wave velocity estimation using linear regression. (Figure from paper IV) @IEEE2019

Summary of presented work

I. Detection of Regional Mechanical Activation of the Left Ventricle using High Frame Rate Ultrasound Imaging

Kaja F. Kvåle, Jørn Bersvendsen, Pål H. Brekke, Sebastien Salles, Espen W. Remme, John M. Aalen, Thor Edvardsen, Eigil Samset, *IEEE Transactions on Medical Imaging, 2019*

In this paper, we assess the first, second and fourth of the aims of study laid out in section 1.2, by investigating the possibilities of using high frame rate ultrasound imaging with a clinical scanner to detect the source of pacing in an animal study. Novel methods for analysis of high frame rate ultrasound data were developed and tested, and the novel signal processing method CFWI was used for this. The context of this study is that arrhythmias occurring in the ventricles are often surgically treated with ablation. For this procedure, a catheter is used to remove the tissue causing the arrhythmia. Locating the correct area can be time consuming as the process consists of invasively probing the heart with an electrode to map the electrical activation. The development of a quick, non-invasive method for visualizing the electrical activity of the heart would therefore be extremely useful for clinicians. From a mechanical activation map it is possible to also see the electrical activation pattern as both waves have been shown to follow the same propagation paths. This study therefore aimed to investigate the feasibility of the developed method to create a spatiotemporal map of the mechanical activation propagation for the purpose of creating a tool to visualize the propagation of electrical activation non-invasively.

For this study, arrhythmias were simulated by pacing the hearts of five open chest animals under anesthesia from several different locations. In addition to the pacing electrodes, combined electromyography (EMG) and sonomicrometry crystals were implanted in the left ventricle (LV). The EMG crystals measured the timing of electrical depolarization at two locations of the heart, and the sonomicrometric crystals measured the distance between crystal pairs which was used to assess the timing of mechanical activation. High frame rate ultrasound data and recordings from the crystals were acquired during pacing.

The ultrasound data was analyzed using the developed method to identify the source of pacing and the propagation pattern of mechanical activation, and the result was visualized in a spatiotemporal isochrone map. The isochrone maps showed the same mechanical activation sequence as the sonomicrometry crystals in 90% of the cases. For electrical activation, the activation sequences from ultrasound were the same as measured with the EMGs in 92% of the cases. Additionally, a coefficient of determination between the activation delay measured with EMG and ultrasound was $R^2 = 0.79$, indicating a strong correlation.

II. Detection of Tissue Fibrosis using Natural Mechanical Wave Velocity Estimation: Feasibility Study

Kaja F. Kvåle, Sebastien Salles, Lars Christian N. Lervik, Asbjørn Støylen, Lasse Løvstakken, Eigil Samset, Hans Torp, *Elsevier Ultrasound in Medicine & Biology 2019*,

In this paper, we assess the first, third and fourth of the study aims laid out in section 1.2, by developing and testing a method, based on CFWI, for mechanical wave propagation velocity estimation from high frame ultrasound data. The developed method was used to analyze ultrasound data from 10 healthy persons, and ultrasound and magnetic resonance imaging (MRI) data from 20 patients with known infarcts. The context of the study is that myocardial fibrosis develops after a myocardial infarct and alters the conduction ability of the tissue and therefore the ability of the heart muscle to contract. Additionally, the fibrous tissue is stiffer than healthy tissue because of the higher

concentration of collagen. Increased tissue stiffness could also occur at earlier stages of ischemic heart disease, before an infarct develops. Therefore, being able to non-invasively characterize tissue stiffness would be beneficial for clinicians for localization of fibrosis and other regions of increased tissue stiffness.

In this feasibility study we estimated the propagation velocity of one specific mechanical wave occurring around the time of the atrial kick and the P-wave of the ECG. The CFWI method was used to estimate motion and acceleration, and the propagation velocity of the mechanical wave was estimated automatically for every spatial point of the LV by tracking the propagation of the wave front from a spatiotemporal map of peak (CFWI) acceleration. The velocities obtained from patients were compared to velocities obtained from the controls, and a positive fibrosis find in the patient results was defined based on the velocities from the controls. Regions of high velocity discovered in patients with high frame rate ultrasound were then compared to locations of fibrosis identified with MRI, and a sensitivity between the methods of 60% was achieved for all infarcts larger than 10% of a segment of the left ventricle. Additionally, the stability of the estimated propagation velocity was evaluated for all subjects and found to be stable through several heart cycles.

III. Comparison of two methods for mechanical activation detection using high frame rate ultrasound imaging

Kaja F. Kvåle, Sebastien Salles, Pål H. Brekke, Thor Edvardsen, Eigil Samset, *Proceeding, 2019 IEEE International Ultrasonics Symposium (IUS)*

The mechanical activation wave detection method developed for paper I was compared to our implementation of the EWI method, and they were both evaluated for feasibility, simplicity, time consumption and accuracy against two invasive reference standards. The same animal model as for paper I was used, including three anesthetized, open chest dogs with implanted combined sonomicrometry and electromyography (EMG) crystals. High frame rate ultrasound data was acquired while the animals were being paced from specified locations of the heart, and mechanical activation isochrone maps were generated using both methods. Additionally, manual measurements of the delay in mechanical activation from the septum to the lateral wall were taken, for comparison against the activation delays measured with sonomicrometry and EMG.

The resulting isochrone maps showed similar locations for the origins of pacing, and for the pattern of propagation for the mechanical activation. However, the isochrones generated by the CFWI method were simpler to interpret due to less noise. Additionally, the CFWI method was found to be less time consuming than the EWI method, mostly due to the time consumption of tissue velocity estimation using Tissue Doppler Imaging (TDI). The coefficients of determination between the activation delay measured with ultrasound vs EMG and sonomicrometry were all above $R^2 = 0.84$, indicating a strong correlation for both methods, but the EWI method had a slightly better accuracy, especially against the mechanical activation delay measured with sonomicrometry. This study showed that there are benefits and limitations to each method.

IV. Velocity estimation of naturally occurring mechanical waves in the left ventricle in healthy persons

Kaja F. Kvåle, Sebastien Salles, Pål H. Brekke, Thor Edvardsen, Eigil Samset, *Proceeding, 2019 IEEE International Ultrasonics Symposium (IUS)*

For this paper, the propagation velocities of three naturally occurring mechanical waves in the left ventricle were investigated for seven healthy volunteers. The context of the study is that there are few

published studies on the velocities of naturally occurring mechanical waves, so this paper aimed to contribute to this field with measurements of normal propagation velocities for different mechanical waves. The aim of this field is to be able to use propagation velocities as an indicator for pathology, but for this to be achieved, knowing the range of normal velocities for healthy persons is necessary. How propagation velocities changed with increasing acquisition frame rate and for different locations of the LV was also investigated.

The approach used for velocity estimation was similar to the method developed for paper II, using the CFWI method to calculate a spatiotemporal (CFWI) acceleration map. For this paper, however, an anatomical trace following the LV walls was drawn by hand on the image, and the coordinates were used to create an anatomical M-mode trace. The CFWI acceleration M-mode map was used for linear regression analysis to find the slope, and thereby, the propagation velocity of the waves. This study found that the lower frame rate intervals led to fewer estimates below the exclusion criteria, and narrower ranges of average velocities between subjects. No pattern was found for increased or decreased propagation velocities in different parts of the LV.

Discussion

4.1 Contributions

In this thesis, contributions have been made in the field of mechanical wave propagation and velocity estimation. This has been applied in two different scenarios. Firstly, two studies concerning the mechanical activation wave in the left ventricle (LV) were performed (papers I and III). Secondly, two studies concerning mechanical wave velocity estimation were performed (papers II and IV). The contributions will be evaluated separately in the following two sections.

4.1.1 Estimation of mechanical activation wave propagation patterns

An almost fully automatic method to track and visualize regional propagation of the mechanical activation wave from 2D high frame rate ultrasound data has been developed, and its feasibility has been tested and validated against invasive measurements, and demonstrated in an animal study (paper I). To be able to visualize the electrical activation non-invasively has long been a sought-after application for clinicians, as identifying abnormal conduction patterns would be of significance for diagnosing many different pathologies, including tissue fibrosis and different arrhythmias. Additionally, being able to detect the source of an arrhythmia with a simple and quick method could be a powerful tool in the ablation treatment for arrhythmias. The presented method therefore has the potential to make a very valuable contribution to clinical practice.

The field of mechanical activation mapping using ultrasound has been studied fairly well. In 2006, Deffieux *et al*., introduced ultrafast plane wave imaging to the field of mechanical wave imaging, and made acquisitions of activation waves propagating in human biceps following electrical stimulation [52]. Then, Couade *et al*. performed the first experiments of ultrafast imaging of activation waves in a single heartbeat in sheep [53]. However, most contributions to this field have been made by the research group of E. Konofagou at Columbia University (New York, USA), where the method called Electromechanical Wave Imaging (EWI) was developed to detect what they have termed the electromechanical wave. For the third project of this paper, a version of EWI (using Tissue Doppler Imaging (TDI) instead of cross correlation for tissue displacement estimation) was implemented to compare its feasibility to our Clutter Filter Wave Imaging (CFWI) based method and against invasive measurements. The results showed that EWI had a very good accuracy against the invasive reference standard, especially for manual measurements where the mechanical activation (zero-crossing of the strain rate curve) was manually defined. However, for automatic mechanical activation detection, we were not able to recreate the results with sufficient accuracy. This was most likely because of two main reasons: firstly, strain rate is the spatial derivative of tissue velocity and is susceptible to noise [54], thus it can cause the trace to have several zero crossings; secondly, even for a very clean strain rate trace, there were occurrences of several zero-crossings in the correct time interval, and sometimes none at all. For an experienced eye, reading the trace and determining if the features stemmed from noise or from actual myocardial movement, and thereby finding the most likely time of activation, was a fairly simple task. However, implementing this experience as a computer algorithm proved to be very challenging. The reported result of EWI is a spatiotemporal isochrone map of the mechanical activation. Generating a readable map without noise or large discontinuities in timing required a lot of filtering and smoothing in addition to manual correction. Thus, it is the experience from this thesis that obtaining a very spatially detailed map of the mechanical activation with accurate information remains very challenging and labor-intensive.

In addition to the difficulty of developing a method for mechanical activation detection, the mechanical activation remains a challenging topic in itself. This is firstly due to the very short duration of the activation in time during which several other events occur almost simultaneously, such as the closure of the mitral valve and movement of blood in the ventricles. Secondly, the definition of mechanical activation is not straight-forward. As mentioned in chapter 2.1, there is a difference

between the active force generation of a segment and the onset of shortening [13]. Onset of active force generation is the first mechanical sign of actin-myosin interaction, and it is independent of loading conditions and contractility. In contrast, onset shortening is load dependent, thus, these definitions of mechanical activation could give different activation maps for the same data. Finally, the activation pattern is very complex as the electrical impulse depolarizes the LV from many locations simultaneously within the same tissue layer, but also spreads to surrounding tissue layers.

Our proposed method is based on the CFWI signal processing method described in section 2.4.1. In paper I, we showed that we were able to use the developed technique to differentiate between activation patterns generated by pacing the heart from different locations (RV, LV and septum), and to approximately identify the locations of pacing. Mechanical activation in our method was defined as the time of peak (CFWI) acceleration, after the (CFWI) velocity had reached a certain set threshold which approximately corresponded to the time of mitral valve closure. The fixed threshold is a weakness of the method because for all investigated spatial points where the velocity trace reached the threshold within the correct temporal interval, a mechanical activation was found. This makes the method vulnerable to tracking the wrong point and not the actual wave front. Noisy areas were also found in the isochrones obtained from the CFWI method, however, less smoothing was required in order to obtain a readable activation map.

One major limitation for both studies (papers I and III) was the low number of included subjects. In line with the principle of "replacement, reduction and refinement", the animals were part of multiple studies and the number of included animals was kept low. Another limitation was the data acquisition of the invasive reference standard. The crystals used for comparison for the ultrasound results had a substantially poorer resolution in space as activation was measured for some locations and segments of the LV only, while mechanical activation was estimated for each spatial point of the LV for the ultrasound data. Furthermore, we have attempted to describe a 3D phenomenon with 2D imaging using only 1D motion estimation. This makes the studies vulnerable, as the mechanical activation wave will propagate in and out of the selected imaging plane. Future work should consist of testing this method for a study group of humans with controlled pacing. This project is ongoing but will not be in the scope of this thesis.

4.1.2 Estimation of mechanical wave propagation velocities

Two studies were performed to evaluate the velocities of naturally occurring mechanical waves. The aim of the first study (paper II) was to investigate the feasibility of using increased propagation velocity as a clinical indicator for cardiac fibrosis by correlating regions of elevated velocity found with ultrasound, to infarct locations found with MRI, in infarct patients. The aim of paper IV was to contribute to the field of mechanical wave velocity estimation with results of velocities found from healthy persons for several different mechanical waves and locations of the LV. The velocity of naturally occurring mechanical waves in the LV is a potential indicator of myocardial stiffness. Tissue fibrosis is known to increase tissue stiffness [55], thus increased mechanical wave velocity is also a possible indicator of fibrosis. The presented methods of this thesis and the results from the performed studies are therefore valuable contributions to a potential novel diagnostic tool for tissue fibrosis.

The mechanical waves studied for these projects (atrial kick, mitral valve closure and aortic valve closure) are thought to propagate as shear waves. Shear wave imaging is a fairly novel approach for evaluating tissue elasticity and stiffness and it is based on high frame rate imaging. The technique has already been demonstrated for detection of tumors and increased tissue stiffness in breast [28, 56-58] and liver [59-61], and studies on these organs are now fairly common. For the heart, although mitral valve closure (MVC) and aortic valve closure (AVC) waves have been described separately in literature [23, 62], studies measuring several waves jointly for the same data set have been limited to animal studies and small human populations [46]. Santos et.al. measured the velocities of MVC and AVC waves jointly in healthy human myocardium in 2018 [46]. The discovered trend was a higher

velocity of the AVC than MVC wave, although the velocities did vary among subjects. This is consistent with the result from this thesis (paper IV), and with theory as the pressure is higher at end-systole than end-diastole as a result of contraction. Additionally, they found that the trend is consistent with previous studies using naturally occurring waves [45], but also acoustically [63, 64] and mechanically [65] induced waves.

The potential of increased natural wave velocity as an indicator of abnormal myocardial states has been reported in literature several times. Santos *et al*. reported results of increased velocities in two patients with known increased myocardial stiffness [46], and the same group later confirmed this in a larger study of the same patient group, in addition to finding a relationship between increased velocities and age [47]. In addition to pathology, aging is known to be associated with increased myocardial stiffness [66], and their results therefore indicate that increased stiffness and high velocities are related. This relationship has been confirmed invasively in an animal study by another group for the mechanical wave following atrial contraction [67]. The same group later showed increased velocities for two patient groups with known increased stiffness compared to healthy persons [68]. For our study of the same wave (paper II), results showed that we were able to correctly identify 60% of locations of known fibrosis in patients using elevated velocity as an indicator.

A limitation of some of the described studies [46, 47] was that the velocity was estimated for the septum only. Our studies have partially mitigated this by measuring the velocities for three apical 2D views resulting in six walls of the LV. However, the experience from our studies is that using 3D data would be beneficial as we were not able to detect if the waves propagated in and out of the imaged planes. The method used for analysis in the described studies were based on TDI, whereas our method was based on CFWI. For our study (paper II), we found that TDI, for our data set, did not give tissue acceleration maps that were of sufficient quality for velocity estimation. The higher SNR of the CFWI method was mainly a result of the clutter filter removing the clutter noise in the near field of the ultrasound beam. Furthermore, some of the described studies report reproducibility as a limitation of their method as the velocities were obtained from manually drawing the slope of the wave in an M-mode image. For our studies, this slope was automatically detected and velocities found by linear regression, which possibly increases reproducibility. Nevertheless, there were several limitations of the methods developed for this thesis. Firstly, for paper II, mechanical wave velocity values were estimated for all imaged spatial points and averaged to find one velocity value per wall. No segmentation was performed which means that regions outside of the cardiac walls probably contributed to the velocity estimate. This is also a possible limitation for paper IV where anatomical traces of the cardiac walls were manually drawn in the image. Secondly, the high pass filter of the CFWI method was kept constant (changed only for the estimation of different waves). Differences in the tissue velocities between different subjects and locations of the LV were observed, therefore, the method would probably benefit from an adaptive cutoff velocity approach. Thirdly, while the waves originating from the valve closures have been determined shear waves with some certainty [46, 47], the origin and type of the wave occurring slightly after the atrial contraction is more uncertain. One hypothesis is that the wave is a shear wave and stems from the force of the atrial kick. Another, that a pressure wave propagating inside the LV could induce the motion on the walls, in the same manner as a pulse wave propagating in an artery [69]. In the pressure wave scenario, the thickness of the ventricular walls and the radius of the LV must be considered to estimate myocardial tissue stiffness. Finally, a small sample size was used, especially for paper IV (where $n = 7$). The study was intended as a contribution to data on normal velocities for healthy persons, to use as a reference to detect pathology. For the wave velocity values to have clinical significance, studies of normal velocities should be conducted in larger populations.

4.2 Evaluation of the high frame rate modality and data acquisition

All contributions in this thesis have been based on high frame rate ultrasound imaging acquired with clinically approved GE Vivid E95 and E9 scanners, with acquisition frame rates ranging from 1000 to 1800 frames per second. The method is based on broad beam acquisition combined with parallel receive beamforming to increase frame rate (described in section 2.3).

For papers I, III and IV, four to six plane waves steered in equidistant directions were transmitted to create a high frame rate image without any compounding. This made the image present with apparent discontinuities between each acquisition sector [70], caused by the asymmetric two-way beams of the parallel beamforming approach [71]. To avoid errors related to this, it was attempted during data acquisition to keep the cardiac walls within one sector, but because of the low spatial resolution of the high frame rate images, image optimization during acquisition was challenging. For paper II, broadly focused beams were used to image the two 20 degrees outermost subsectors of the image sector only, using manual adjustment to cover the left ventricular walls within the two subsectors [23]. The data for this project were collected prior to the start of this thesis, but the problem remained the same, keeping the cardiac walls within sectors during image acquisition.

For all studies, the image acquisition was challenging because the high frame rate imaging modality displayed images that were difficult to interpret, especially at the higher frame rates. It was therefore not possible to ensure that the exact same view and tissue had been imaged for every subject, nor was it possible to know that the cardiac walls were completely in focus during image acquisition. Thus, there is room for improvement of the imaging technique, especially the pre-processing of the frames, for it to be clinically applicable.

4.3 Evaluation of the CFWI method

Three of the four mechanical wave detection methods developed for this thesis were based on the same underlying approach for tissue motion and acceleration estimation (CFWI, described in section 2.4.1). The clutter filter approach was originally developed by Salles *et al*. [49, 50], who have also applied this method to 3D echocardiographic sequences [72].

All approaches to mechanical wave detection involve two major steps: tissue motion estimation, and mechanical wave velocity or propagation pattern detection. The two main techniques used for axial tissue motion estimation are phase-based, such as TDI, and RF/B-mode cross correlation (CC). TDI is a computationally inexpensive approach compared to CC techniques, but it is sensitive to beam angle and aliasing [73], contrary to CC methods. The TDI approach (described in section 2.2.5) was used as a comparison to the CFWI method for paper III.

S. Salles *et al*. evaluated CFWI, and TDI for comparison, for three mechanical wave applications – one in a tissue mimicking phantom, and two *in vivo*. The *in vivo* experiments were on the pulse wave in the carotid artery, and on naturally occurring waves in the left ventricle [49, 50]. For a fair comparison, all smoothing filters used were the same for CFWI and TDI. The experiments found that CFWI was better able to visualize the shear wave propagation along depth and time for the tissue mimicking phantom. For the *in vivo* experiments, mechanical wave velocity was estimated using the acceleration M-mode maps for both methods. It was shown that the mechanical wave velocities obtained with CFWI were more consistent than those obtained with TDI, explained by the fact that the temporal resolution and signal-to-noise ratio (SNR) of the slope (wave) was found to be superior with CFWI. Additionally, for the mechanical waves of the LV, better SNR was found in the apical and lateral wall regions of the LV, especially. The same result was found for paper II in this thesis because the clutter filter removes noise in the near field of the ultrasound beam as mentioned in the previous section. Thus, CFWI seems to be more sensitive to small motion induced by the mechanical waves, which is important because of the reduced image quality of high frame rate sequences.

The CFWI method is not able to differentiate between mechanical waves induced by a positive or negative velocity, only the locality of tissue velocity induced by the mechanical wave is detected. Thus, to understand the direction of the tissue motion, the tissue velocity will need to be estimated. Nevertheless, even if the tissue velocities themselves could be clinically useful, only the locality of the tissue velocity is needed to be able to detect the mechanical waves and estimate the propagation velocity. However, the tissue velocity of interest will need to be determined for a given application, to be able to set the cutoff velocity correctly and use the filter properly.

4.4 Differences in methodologies

Mechanical and electrical activation

The first clinical aim of this thesis was to map and visualize the electrical and mechanical activation of the LV. Currently, in clinical practice, noninvasive detection and diagnosis of cardiac electrical activity is performed with a 12-lead ECG which measures electrical activity on the surface of the body and has a limited spatial resolution [38]. To overcome this, electrocardiographic imaging (ECGI) was developed to map the electrical activity at high spatial resolution [74, 75]. ECGI consists of measuring electricity on the body surface using strips or a multi-electrode vest, then to retrieve the heart-torso geometry using a CT or MRI scan, and finally, to combine the information using a mathematical model to recreate a map of the electrical activity of the heart [75]. This technique has been shown to be useful for decreasing the time spent on the ablation procedure, but the results of the method have been shown to depend considerably on implementation choices [76]. Compared to ultrasound it is also time consuming and requires extra equipment, in addition to the added radiation exposure from the CT scan to the patient. Furthermore, a method called MR tagging has been developed to non-invasively map mechanical activity of the LV [77], but is currently limited by low frame rate [6]. Invasive procedures currently employed in the clinic are typically catheter-based, such as electrophysiology contact mapping [16, 78]. This procedure results in ionizing exposure, prolonged sedation or anesthesia, risk of complications and arrhythmias for the patient, in addition to being time consuming and costly [42].

Tissue stiffness and fibrosis detection

The second clinical aim of this thesis was to detect locations in the LV of increased tissue stiffness and fibrosis. Invasive procedures of fibrosis detection currently applied in the clinic are biomarkers from myocardial biopsies and blood tests [19]. Histological analysis of the volume fraction of collagen in the biopsy is regarded as the gold standard for fibrosis detection [79, 80], and with this method the total collagen can be quantified, and the type and the extent of fibrosis can be described. The limitations of this method are the purely local assessment, the limited amount of tissue tested and the procedure-related risk [81].

For non-invasive fibrosis detection, MRI is considered the gold standard [82]. Fibrosis can also be accurately detected with a cardiac computed tomography (CT) scan, but it is rarely used due to the radiation hazard [83]. MRI gives the advantage over echocardiography that it is possible to accurately find the size of a fibrous tissue region [84]. However, before fibrosis develops, it has been shown that the tissue stiffness can be increased at an earlier stage in the development of disease [85, 86]. This cannot necessarily be detected with MRI, while for ultrasound it is possible with the new methods proposed in this thesis, and with shear wave imaging [87, 88]. Furthermore, increased myocardial reflectivity in ultrasound images has been proposed as a marker for fibrosis [89].

4.5 Future perspectives and further work

This thesis aimed to contribute to the development and testing of new methods for analysis of high frame rate ultrasound data. The field of high frame rate ultrasound research is a fast developing one, and development of techniques for even higher frame rates, improved image quality and new applications that can take advantage of the increased load of information, are still under investigation. The extensive research on high frame rate imaging, has however, already resulted in new ultrasonic imaging modes including shear wave elastography, electromechanical wave imaging, ultrafast Doppler, ultrafast contrast imaging, and even functional ultrasound imaging of brain activity. Thus, these techniques have surpassed the research phase and are now entering the clinical medical ultrasound community.

For the methods developed for this thesis, a significant improvement would be to expand them to high frame rate volume data. 3D imaging has been limited to very low frame rates, or to the creation of higher frame rates by acquiring data over several heart cycles, which requires the patient to have a stable heart rhythm.

The studies in this thesis have been focused on the LV only, however, our developed methods could be of use for studying and diagnosing pathologies related to abnormal conduction and increased tissue stiffness in other chambers of the heart as well. An example of use is the assessment of the most common arrhythmia, atrial fibrillation [90], as it is often treated with ablation and is known to be associated with diffuse fibrosis [91]. The atria have thinner walls and are smaller in size compared to the LV, which makes detection of mechanical waves more challenging, but it is likely that it is feasible and should be investigated in future work. Furthermore, the assessment of diastolic cardiac function with echocardiography is currently complex and based on several measured parameters [92]. Another example of use of our methods is the investigation of increased diastolic myocardial stiffness as an indicator of LV diastolic function.

Conclusions

In this thesis, four papers (two in journals and two conference proceedings) have been presented to cover the four main goals laid out in section 1.2.

The first goal of this thesis was to investigate the clinical possibilities of high frame rate ultrasound imaging for pathology detection and to develop methods for analysis for this novel imaging modality. To achieve this goal, four different studies have been performed and three new methods for data analysis have been developed. Three of the four studies were directly related to pathology and methods using high frame rate imaging were developed for all contributions.

Our methods have been evaluated for several different clinical scenarios and tested and validated against invasive reference standards. More specifically, the second goal of this thesis was to develop and test a method for regional mechanical activation detection for the purpose of locating sources of arrhythmias. To achieve this goal, two studies were performed on data from an animal study where it was shown that our developed method was able to approximately locate sources of pacing and detect the propagation pattern of mechanical activation. Furthermore, our method was shown to have a good accuracy against the invasive reference standard used. The method developed for Paper I was further validated against a more conventional ultrasound method for activation detection in paper III.

Our third goal of developing a method for natural mechanical wave detection for the purpose of fibrosis detection was achieved in a study that correlated locations of fibrosis found using our method to locations of fibrosis found with MRI. An adequate sensitivity of the two methods of 60% was found with some regional differences in the LV. Another important result from this feasibility study was that the investigated mechanical wave was found to have a stable propagation velocity through several heart cycles. This could indicate that this phenomenon could be useful for detecting pathology through abnormal velocities. An additional study in this field was the investigation of mechanical wave velocities from healthy persons which contributed to increased knowledge of the range of normal propagation velocities for several different waves, the relation of velocity to increasing frame rates and location in the LV.

Through the above mentioned studies we have achieved our fourth goal of testing clutter filter wave imaging (CFWI) for detection of mechanical waves. The CFWI approach was used for all studies in this thesis and we have successfully applied this technique to estimate both propagation velocity and pattern for four different waves in the LV.

Bibliography

[1] W. H. Organization, "Global Health Estimates 2016: Deaths by Cause, Age, Sex, by Country and by Region, 2000-2016. Geneva, World Health Organization," 2018.

[2] E. Wilkins *et al.*, "European cardiovascular disease statistics 2017," 2017.

[3] E. Macé, G. Montaldo, I. Cohen, M. Baulac, M. Fink, and M. Tanter, "Functional ultrasound imaging of the brain," *Nature methods*, vol. 8, no. 8, p. 662, 2011.

[4] J. Bercoff *et al.*, "Ultrafast compound Doppler imaging: Providing full blood flow characterization," *IEEE transactions on ultrasonics, ferroelectrics, and frequency control*, vol. 58, no. 1, pp. 134-147, 2011.

[5] M. Tanter and M. Fink, "Ultrafast imaging in biomedical ultrasound," *IEEE transactions on ultrasonics, ferroelectrics, and frequency control*, vol. 61, no. 1, pp. 102-119, 2014.

[6] D. A. Auger *et al.*, "Imaging left-ventricular mechanical activation in heart failure patients using cine DENSE MRI: Validation and implications for cardiac resynchronization therapy," *Journal of Magnetic Resonance Imaging*, vol. 46, no. 3, pp. 887-896, 2017.

[7] J. Provost *et al.*, "Electromechanical wave imaging for arrhythmias," *Physics in Medicine & Biology*, vol. 56, no. 22, p. L1, 2011.

[8] J. Pinnell, S. Turner, and S. Howell, "Cardiac muscle physiology," *Continuing Education in Anaesthesia, Critical Care and Pain*, vol. 7, no. 3, pp. 85-88, 2007.

[9] K. A. Y. J. Gordon Betts, James A. Wise, Eddie Johnson, Brandon Poe, Dean H. Kruse, Oksana Korol, Jody E. Johnson, Mark Womble, Peter DeSaix, *Anatomy and Physiology*, OpenStax: OpenStax, 2013. [Online]. Available: https://openstax.org/books/anatomy-and-physiology/pages/1-introduction.

[10] R. E. Ideker, W. Kong, and S. Pogwizd, "Purkinje fibers and arrhythmias," *Pacing and clinical electrophysiology: PACE*, vol. 32, no. 3, p. 283, 2009.

[11] F. Prinzen, C. Augustijn, M. Allessie, T. Arts, T. Delhass, and R. Reneman, "The time sequence of electrical and mechanical activation during spontaneous beating and ectopic stimulation," *European heart journal*, vol. 13, no. 4, pp. 535-543, 1992.

[12] O. A. Smiseth and E. W. Remme, "Regional left ventricular electric and mechanical activation and relaxation," ed: Journal of the American College of Cardiology, 2006.

[13] K. Russell *et al.*, "Evaluation of left ventricular dyssynchrony by onset of active myocardial force generation: a novel method that differentiates between electrical and mechanical etiologies," *Circulation: Cardiovascular Imaging*, vol. 3, no. 4, p. 405, 2010.

[14] A. Costet *et al.*, "Non-invasive characterization of focal arrhythmia with electromechanical wave imaging in vivo," *Ultrasound in medicine & biology*, vol. 44, no. 11, pp. 2241-2249, 2018.

[15] L. Melki *et al.*, "Localization of Accessory Pathways in Pediatric Patients With Wolff-Parkinson-White Syndrome Using 3D-Rendered Electromechanical Wave Imaging," *JACC: Clinical Electrophysiology*, 2019.

[16] A. Schratter, G. Delle Karth, and R. Achleitner, "Ablation of Ischemic Ventricular Tachycardia Using a Multipolar Catheter and 3-dimensional Mapping System for High-density Electro-anatomical Reconstruction," *JoVE (Journal of Visualized Experiments)*, no. 143, p. e57234, 2019.

[17] D. V. Cokkinos, C. Pantos, G. Heusch, and H. Taegtmeyer, *Myocardial ischemia: from mechanisms to therapeutic potentials*. Springer Science & Business Media, 2006.

[18] M. Nathan, L. C. Ying, C. Pierre, B. David, and L. João, "Assessment of myocardial fibrosis with cardiac magnetic resonance," *Journal of the American college of cardiology*, vol. 57, no. 8, p. 891, 2011.

[19] T. Espeland, I. G. Lunde, L. Gullestad, and S. Aakhus, "Myocardial fibrosis," *Tidsskrift for den Norske laegeforening: tidsskrift for praktisk medicin, ny raekke*, vol. 138, no. 16, 2018.

[20] A. J. Fischetti and R. C. Scott, "Basic ultrasound beam formation and instrumentation," *Clinical techniques in small animal practice*, vol. 22, no. 3, pp. 90-92, 2007.

[21] N. blog. https://www.nuemblog.com/ (accessed.

[22] A. Ng and J. Swanevelder, "Resolution in ultrasound imaging," *Continuing Education in Anaesthesia Critical Care & Pain*, vol. 11, no. 5, pp. 186-192, 2011, doi: 10.1093/bjaceaccp/mkr030.
[23] B. Brekke *et al.*, "Ultra-high frame rate tissue Doppler imaging," *Ultrasound in medicine & biology*, vol. 40, no. 1, pp. 222-231, 2014.
[24] F. Viola and W. F. Walker, "A comparison of the performance of time-delay estimators in medical ultrasound," *IEEE transactions on ultrasonics, ferroelectrics, and frequency control*, vol. 50, no. 4, pp. 392-401, 2003.
[25] M. Couade, "The advent of ultrafast ultrasound in vascular imaging: a review," *Journal of Vascular Diagnostics and Interventions*, vol. 4, p. 9, 2016.
[26] M. Tanter, J. Bercoff, L. Sandrin, and M. Fink, "Ultrafast compound imaging for 2-D motion vector estimation: Application to transient elastography," *IEEE transactions on ultrasonics, ferroelectrics, and frequency control*, vol. 49, no. 10, pp. 1363-1374, 2002.
[27] L. Sandrin, M. Tanter, S. Catheline, and M. Fink, "Shear modulus imaging with 2-D transient elastography," *IEEE transactions on ultrasonics, ferroelectrics, and frequency control*, vol. 49, no. 4, pp. 426-435, 2002.
[28] J. Bercoff *et al.*, "In vivo breast tumor detection using transient elastography," *Ultrasound in medicine & biology*, vol. 29, no. 10, pp. 1387-1396, 2003.
[29] J. R. Doherty, G. E. Trahey, K. R. Nightingale, and M. L. Palmeri, "Acoustic radiation force elasticity imaging in diagnostic ultrasound," *IEEE transactions on ultrasonics, ferroelectrics, and frequency control*, vol. 60, no. 4, pp. 685-701, 2013.
[30] H. Kanai, "Propagation of spontaneously actuated pulsive vibration in human heart wall and in vivo viscoelasticity estimation," *IEEE transactions on ultrasonics, ferroelectrics, and frequency control*, vol. 52, no. 11, pp. 1931-1942, 2005.
[31] H. Kanai, "Propagation of vibration caused by electrical excitation in the normal human heart," *Ultrasound in medicine & biology*, vol. 35, no. 6, pp. 936-948, 2009.
[32] H. Kanai and Y. Koiwa, "Myocardial rapid velocity distribution," *Ultrasound in medicine & biology*, vol. 27, no. 4, pp. 481-498, 2001.
[33] Y. Koiwa, H. Kanai, H. Hasegawa, Y. Saitoh, and K. Shirato, "Left ventricular transmural systolic function by high-sensitivity velocity measurement “phased-tracking method” across the septum in doxorubicin cardiomyopathy," *Ultrasound in medicine & biology*, vol. 28, no. 11-12, pp. 1395-1403, 2002.
[34] J. Provost, W.-N. Lee, K. Fujikura, and E. E. Konofagou, "Imaging the electromechanical activity of the heart in vivo," *Proceedings of the National Academy of Sciences*, vol. 108, no. 21, pp. 8565-8570, 2011.
[35] M. Pernot and E. E. Konofagou, "Electromechanical imaging of the myocardium at normal and pathological states," in *IEEE Ultrasonics Symposium, 2005.*, 2005, vol. 2: IEEE, pp. 1091-1094.
[36] M. Pernot, K. Fujikura, S. D. Fung-Kee-Fung, and E. E. Konofagou, "ECG-gated, mechanical and electromechanical wave imaging of cardiovascular tissues in vivo," *Ultrasound in medicine & biology*, vol. 33, no. 7, pp. 1075-1085, 2007.
[37] E. E. Konofagou, J. Luo, D. Saluja, D. O. Cervantes, J. Coromilas, and K. Fujikura, "Noninvasive electromechanical wave imaging and conduction-relevant velocity estimation in vivo," *Ultrasonics*, vol. 50, no. 2, pp. 208-215, 2010.
[38] J. Provost, A. Gambhir, J. Vest, H. Garan, and E. E. Konofagou, "A clinical feasibility study of atrial and ventricular electromechanical wave imaging," *Heart Rhythm*, vol. 10, no. 6, pp. 856-862, 2013.
[39] J. Provost, S. Thiébaut, J. Luo, and E. E. Konofagou, "Single-heartbeat electromechanical wave imaging with optimal strain estimation using temporally unequispaced acquisition sequences," *Physics in Medicine & Biology*, vol. 57, no. 4, p. 1095, 2012.
[40] J. Provost, W.-N. Lee, K. Fujikura, and E. E. Konofagou, "Electromechanical wave imaging of normal and ischemic hearts in vivo," *IEEE transactions on medical imaging*, vol. 29, no. 3, pp. 625-635, 2010.

[41] J. Provost *et al.*, "Assessing the atrial electromechanical coupling during atrial focal tachycardia, flutter, and fibrillation using electromechanical wave imaging in humans," *Computers in biology and medicine,* vol. 65, pp. 161-167, 2015.
[42] A. Costet *et al.*, "Electromechanical wave imaging of biologically and electrically paced canine hearts in vivo," *Ultrasound in medicine & biology,* vol. 40, no. 1, pp. 177-187, 2014.
[43] J. Grondin *et al.*, "Validation of electromechanical wave imaging in a canine model during pacing and sinus rhythm," *Heart rhythm,* vol. 13, no. 11, pp. 2221-2227, 2016.
[44] J.-U. Voigt *et al.*, "Strain rate imaging for the assessment of preload-dependent changes in regional left ventricular diastolic longitudinal function," *Journal of the American Society of Echocardiography,* vol. 15, no. 1, pp. 13-19, 2002.
[45] H. J. Vos *et al.*, "Cardiac shear wave velocity detection in the porcine heart," *Ultrasound in medicine & biology,* vol. 43, no. 4, pp. 753-764, 2017.
[46] P. Santos *et al.*, "Natural shear wave imaging in the human heart: normal values, feasibility and reproducibility," *IEEE transactions on ultrasonics, ferroelectrics, and frequency control,* 2018.
[47] A. Petrescu *et al.*, "Velocities of Naturally Occurring Myocardial Shear Waves Increase With Age and in Cardiac Amyloidosis," *JACC: Cardiovascular Imaging,* 2019.
[48] S. Langeland, J. D'hooge, H. Torp, B. Bijnens, and P. Suetens, "Comparison of time-domain displacement estimators for two-dimensional RF tracking," *Ultrasound in medicine & biology,* vol. 29, no. 8, pp. 1177-1186, 2003.
[49] S. Salles, H. Torp, S. A. Aase, and T. G. Bjåstad, "Clutter filter wave imaging: A new way to visualize and detect mechanical waves propagation," in *Ultrasonics Symposium (IUS), 2017 IEEE International*, 2017: IEEE, pp. 1-4.
[50] S. Salles, L. Løstakken, S. A. Aase, T. G. Bjåstad, and H. Torp, "Clutter Filter Wave Imaging," *IEEE transactions on ultrasonics, ferroelectrics, and frequency control,* 2019.
[51] K. Kvale *et al.*, "Detection of Regional Mechanical Activation of the Left Ventricular Myocardium using High Frame Rate Ultrasound Imaging," *IEEE transactions on medical imaging,* 2019.
[52] T. Deffieux, J.-L. Gennisson, M. Tanter, M. Fink, and A. Nordez, "Ultrafast imaging of in vivo muscle contraction using ultrasound," *Applied physics letters,* vol. 89, no. 18, p. 184107, 2006.
[53] M. Couade *et al.*, "Ultrafast imaging of the heart using circular wave synthetic imaging with phased arrays," in *2009 IEEE International Ultrasonics Symposium*, 2009: IEEE, pp. 515-518.
[54] L. C. N. Lervik *et al.*, "Myocardial Strain Rate by Anatomic Doppler Spectrum: First Clinical Experience Using Retrospective Spectral Tissue Doppler from Ultra-High Frame Rate Imaging," *Ultrasound in medicine & biology,* vol. 43, no. 9, pp. 1919-1929, 2017.
[55] D. A. Kass, J. G. Bronzwaer, and W. J. Paulus, "What mechanisms underlie diastolic dysfunction in heart failure?," *Circulation research,* vol. 94, no. 12, pp. 1533-1542, 2004.
[56] M. Tanter *et al.*, "Quantitative assessment of breast lesion viscoelasticity: initial clinical results using supersonic shear imaging," *Ultrasound in medicine & biology,* vol. 34, no. 9, pp. 1373-1386, 2008.
[57] A. Athanasiou *et al.*, "Breast lesions: quantitative elastography with supersonic shear imaging—preliminary results," *Radiology,* vol. 256, no. 1, pp. 297-303, 2010.
[58] W. A. Berg *et al.*, "Shear-wave elastography improves the specificity of breast US: the BE1 multinational study of 939 masses," *Radiology,* vol. 262, no. 2, pp. 435-449, 2012.
[59] T. Deffieux, G. Montaldo, M. Tanter, and M. Fink, "Shear wave spectroscopy for in vivo quantification of human soft tissues visco-elasticity," *IEEE transactions on medical imaging,* vol. 28, no. 3, pp. 313-322, 2008.
[60] M. Muller, J.-L. Gennisson, T. Deffieux, M. Tanter, and M. Fink, "Quantitative viscoelasticity mapping of human liver using supersonic shear imaging: preliminary in vivo feasability study," *Ultrasound in medicine & biology,* vol. 35, no. 2, pp. 219-229, 2009.
[61] É. Bavu *et al.*, "Noninvasive in vivo liver fibrosis evaluation using supersonic shear imaging: a clinical study on 113 hepatitis C virus patients," *Ultrasound in medicine & biology,* vol. 37, no. 9, pp. 1361-1373, 2011.

[62] P. Santos, E. Samset, and J. D'hooge, "Volumetric imaging of fast mechanical waves in the heart using a clinical ultrasound system," in *2017 IEEE International Ultrasonics Symposium (IUS)*, 2017: IEEE, pp. 1-5.
[63] M. Pernot, M. Couade, P. Mateo, B. Crozatier, R. Fischmeister, and M. Tanter, "Real-time assessment of myocardial contractility using shear wave imaging," *Journal of the American College of Cardiology*, vol. 58, no. 1, pp. 65-72, 2011.
[64] P. J. Hollender, P. D. Wolf, R. Goswami, and G. E. Trahey, "Intracardiac echocardiography measurement of dynamic myocardial stiffness with shear wave velocimetry," *Ultrasound in medicine & biology*, vol. 38, no. 7, pp. 1271-1283, 2012.
[65] M. W. Urban, C. Pislaru, I. Z. Nenadic, R. R. Kinnick, and J. F. Greenleaf, "Measurement of viscoelastic properties of in vivo swine myocardium using lamb wave dispersion ultrasound vibrometry (LDUV)," *IEEE transactions on medical imaging*, vol. 32, no. 2, pp. 247-261, 2013.
[66] E. G. Lakatta and D. Levy, "Arterial and cardiac aging: major shareholders in cardiovascular disease enterprises: Part II: the aging heart in health: links to heart disease," *Circulation*, vol. 107, no. 2, pp. 346-354, 2003.
[67] C. Pislaru, P. A. Pellikka, and S. V. Pislaru, "Wave propagation of myocardial stretch: correlation with myocardial stiffness," *Basic research in cardiology*, vol. 109, no. 6, p. 438, 2014.
[68] C. Pislaru, M. M. Alashry, J. J. Thaden, P. A. Pellikka, M. Enriquez-Sarano, and S. V. Pislaru, "Intrinsic wave propagation of myocardial stretch, a new tool to evaluate myocardial stiffness: a pilot study in patients with aortic stenosis and mitral regurgitation," *Journal of the American Society of Echocardiography*, vol. 30, no. 11, pp. 1070-1080, 2017.
[69] J. Vappou, J. Luo, and E. E. Konofagou, "Pulse wave imaging for noninvasive and quantitative measurement of arterial stiffness in vivo," *American journal of hypertension*, vol. 23, no. 4, pp. 393-398, 2010.
[70] G. Montaldo, M. Tanter, J. Bercoff, N. Benech, and M. Fink, "Coherent plane-wave compounding for very high frame rate ultrasonography and transient elastography," *IEEE transactions on ultrasonics, ferroelectrics, and frequency control*, vol. 56, no. 3, pp. 489-506, 2009.
[71] T. Hergum, T. Bjastad, K. Kristoffersen, and H. Torp, "Parallel beamforming using synthetic transmit beams," *IEEE transactions on ultrasonics, ferroelectrics, and frequency control*, vol. 54, no. 2, pp. 271-280, 2007.
[72] S. Salles, A. Rodriguez-Molares, T. Bjastad, S. A. Aase, and H. Torp, "3D myocardial mechanical wave measurements using high frame rate ultrasound imaging and Clutter filter wave imaging: Towards a 3D myocardial elasticity mapping," in *Ultrasonics Symposium (IUS), 2017 IEEE International*, 2017: IEEE, pp. 1-1.
[73] C. Jia *et al.*, "Comparison of 2-D speckle tracking and tissue Doppler imaging in an isolated rabbit heart model," *IEEE transactions on ultrasonics, ferroelectrics, and frequency control*, vol. 57, no. 11, 2010.
[74] Y. Wang *et al.*, "Noninvasive electroanatomic mapping of human ventricular arrhythmias with electrocardiographic imaging," *Science translational medicine*, vol. 3, no. 98, pp. 98ra84-98ra84, 2011.
[75] C. Ramanathan, R. N. Ghanem, P. Jia, K. Ryu, and Y. Rudy, "Noninvasive electrocardiographic imaging for cardiac electrophysiology and arrhythmia," *Nature medicine*, vol. 10, no. 4, p. 422, 2004.
[76] M. Cluitmans *et al.*, "Validation and opportunities of electrocardiographic imaging: from technical achievements to clinical applications," *Frontiers in physiology*, vol. 9, p. 1305, 2018.
[77] B. T. Wyman, W. C. Hunter, F. W. Prinzen, and E. R. McVeigh, "Mapping propagation of mechanical activation in the paced heart with MRI tagging," *American Journal of Physiology-Heart and Circulatory Physiology*, vol. 276, no. 3, pp. H881-H891, 1999.
[78] F. S. Ng, C. Roney, C. D. Cantwell, and N. S. Peters, "Fundamentals of Cardiac Mapping," *Cardiac Mapping*, p. 70, 2019.

[79] A. Barison, C. Grigoratos, G. Todiere, and G. D. Aquaro, "Myocardial interstitial remodelling in non-ischaemic dilated cardiomyopathy: insights from cardiovascular magnetic resonance," *Heart failure reviews,* vol. 20, no. 6, pp. 731-749, 2015.
[80] R. Everett, C. Stirrat, S. Semple, D. Newby, M. Dweck, and S. Mirsadraee, "Assessment of myocardial fibrosis with T1 mapping MRI," *Clinical Radiology,* vol. 71, no. 8, pp. 768-778, 2016.
[81] P. Pattanayak and D. A. Bleumke, "Tissue characterization of the myocardium: state of the art characterization by magnetic resonance and computed tomography imaging," *Radiologic Clinics,* vol. 53, no. 2, pp. 413-423, 2015.
[82] E. B. Schelbert, G. C. Fonarow, R. O. Bonow, J. Butler, and M. Gheorghiade, "Therapeutic targets in heart failure: refocusing on the myocardial interstitium," *Journal of the American College of Cardiology,* vol. 63, no. 21, pp. 2188-2198, 2014.
[83] S. Badiani, J. van Zalen, T. A. Treibel, S. Bhattacharyya, J. C. Moon, and G. Lloyd, "Aortic stenosis, a left ventricular disease: insights from advanced imaging," *Current cardiology reports,* vol. 18, no. 8, p. 80, 2016.
[84] L. Iles *et al.*, "Evaluation of diffuse myocardial fibrosis in heart failure with cardiac magnetic resonance contrast-enhanced T1 mapping," *Journal of the American College of Cardiology,* vol. 52, no. 19, pp. 1574-1580, 2008.
[85] R. Ventura-Clapier and V. Veksler, "Myocardial ischemic contracture. Metabolites affect rigor tension development and stiffness," *Circulation research,* vol. 74, no. 5, pp. 920-929, 1994.
[86] J. Amano *et al.*, "Effects of myocardial ischemia on regional function and stiffness in conscious dogs," *American Journal of Physiology-Heart and Circulatory Physiology,* vol. 252, no. 1, pp. H110-H117, 1987.
[87] O. Villemain *et al.*, "Myocardial stiffness evaluation using noninvasive shear wave imaging in healthy and hypertrophic cardiomyopathic adults," *JACC: Cardiovascular Imaging,* 2018.
[88] M. Pernot *et al.*, "Shear wave imaging of passive diastolic myocardial stiffness: stunned versus infarcted myocardium," *JACC: Cardiovascular Imaging,* vol. 9, no. 9, pp. 1023-1030, 2016.
[89] D. L. Prior *et al.*, "Calibrated integrated backscatter and myocardial fibrosis in patients undergoing cardiac surgery," *Open heart,* vol. 2, no. 1, p. e000278, 2015.
[90] C. R. Wyndham, "Atrial fibrillation: the most common arrhythmia," *Texas Heart Institute Journal,* vol. 27, no. 3, p. 257, 2000.
[91] I. M. Khurram *et al.*, "Association between left atrial stiffness index and atrial fibrillation recurrence in patients undergoing left atrial ablation," *Circulation: Arrhythmia and Electrophysiology,* vol. 9, no. 3, p. e003163, 2016.
[92] T. Kuznetsova, L. Herbots, Y. Jin, K. Stolarz-Skrzypek, and J. A. Staessen, "Systolic and diastolic left ventricular dysfunction: from risk factors to overt heart failure," *Expert review of cardiovascular therapy,* vol. 8, no. 2, pp. 251-258, 2010.

II. Detection of Tissue Fibrosis using Natural Mechanical Wave Velocity Estimation: Feasibility Study

Ultrasound in Medicine and Biology, 2020

Ultrasound in Med. & Biol., Vol. 46, No. 9, pp. 2481–2492, 2020

0301-5629/$ - see front matter

https://doi.org/10.1016/j.ultrasmedbio.2020.04.022

● *Original Contribution*

DETECTION OF TISSUE FIBROSIS USING NATURAL MECHANICAL WAVE VELOCITY ESTIMATION: FEASIBILITY STUDY

Kaja F. Kvåle,[*,†,‡] Sebastien Salles,[§,¶] Lars Christian N. Lervik,[§] Asbjørn Støylen,[§,‖] Lasse Løvstakken,[§] Eigil Samset,[*,†,‡] and Hans Torp[§]

[*] Center for Cardiological Innovation (CCI), Oslo University Hospital, Oslo, Norway; [†] GE Vingmed Ultrasound, Horten, Norway; [‡] Institute of Informatics, University of Oslo, Oslo, Norway; [§] Department of Circulation and Medical Imaging, Norwegian University of Science and Technology, Trondheim, Norway; [¶] Université de Lyon, INSA-Lyon, Université Claude Bernard Lyon 1, UJM-Saint Etienne, CNRS, Inserm, CREATIS UMR 5220, Lyon, France; and [‖] Department of Cardiology, St. Olavs Hospital, Trondheim, Norway

Abstract—In the feasibility study described here, we developed and tested a novel method for mechanical wave velocity estimation for tissue fibrosis detection in the myocardium. High-frame-rate ultrasound imaging and a novel signal processing method called clutter filter wave imaging was used. A mechanical wave propagating through the left ventricle shortly after the atrial contraction was measured in the three different apical acquisition planes, for 20 infarct patients and 10 healthy controls. The results obtained were correlated with fibrosis locations from magnetic resonance imaging, and a sensitivity ≥60% was achieved for all infarcts larger than 10% of the left ventricle. The stability of the wave through several heart cycles was assessed and found to be of high quality. This method therefore has potential for non-invasive fibrosis detection in the myocardium, but further validation in a larger group of subjects is needed. (E-mail addresses: kaja.kvale@ge.com, kajakvale@gmail.com)

Key Words: **High-frame-rate ultrasound imaging, Mechanical wave velocity estimation, Clutter filter wave imaging, Natural mechanical wave, Fibrosis.**

INTRODUCTION

Myocardial stiffness is known to play a key role in diastolic left ventricular (LV) function (Kass et al. 2004). Moreover, increased myocardial stiffness is associated with many cardiac diseases, including myocardial fibrosis (Nathan et al. 2011). Current non-invasive techniques for myocardial fibrosis detection include contrast-enhanced magnetic resonance imaging (MRI) and echocardiography. MRI has the advantage over echocardiography that it can be used to accurately find the size of a fibrotic tissue region (Iles et al. 2008), but it does not directly measure cardiac function. For echocardiography, increased myocardial reflectivity has been proposed as a marker for LV fibrosis (Prior et al. 2015); otherwise, there are currently no other methods for directly detecting myocardial fibrosis. Several methods have emerged, however, to investigate myocardial function and stiffness, such as tissue Doppler imaging (TDI) and strain imaging (Heimdal et al. 1998; Pislaru et al. 2004; Sutherland et al. 2004), and shear wave imaging (Pernot et al. 2011, 2016). The benefit of assessing myocardial stiffness over myocardial fibrosis is that increased myocardial stiffness occurs at an earlier stage in the disease (Ventura-Clapier and Veksler 1994), which could make it possible to detect fibrosis in an early phase (Amano et al. 1987). Other benefits of ultrasound over MRI are the cost and bedside availability and the fact that echocardiography is already an integral part of routine examination of the patient's heart.

TDI, which measures tissue velocity, could be useful in assessing myocardial stiffness from local variations in velocity, but tethering, which means that contracting tissue will cause neighboring tissue to move, makes it difficult to separate active from passive motion with this method (Lervik et al. 2017). Furthermore, strain imaging is used to assess cardiac deformation (Heimdal et al. 1998; Pislaru et al. 2004). The deformation patterns have been found to correlate with the change in myocardial stiffness, but the technique suffers from large inter-variability depending on the person performing the exam and the equipment used (Dalen et al. 2009). Another

Address correspondence to: Kaja F. Kvåle, Center for Cardiological Innovation (CCI), Sognsnsvannsveien 9, Oslo 0372, Norway. E-mail addresses: kaja.kvale@ge.com, kajakvale@gmail.com

approach introduced for non-invasive assessment of myocardial stiffness is ultrasound shear wave imaging (Kanai et al. 1993), which consists of capturing the transient response of tissue to a local perturbation to derive mechanical properties such as the stiffness and viscosity of the tissue. The local perturbation can be produced artificially such as by a mechanically vibrating source (Urban et al. 2013); can be induced by the radiation force of the ultrasound probe (Pernot et al. 2016); or can occur naturally as a result of different cardiac events, for instance, closure of the valves (Pernot et al. 2007; Kanai 2009; Brekke et al. 2014; Santos et al. 2017; Vos et al. 2017). Artificially produced mechanical waves (MWs) have the advantages of high frequency content and the possibility of estimating stiffness at any time during the cardiac cycle. However, strong attenuation by the tissue makes this method suitable only at shallow depths, for example, in the liver (Ferraioli et al. 2014). Naturally occurring MWs are bound to a certain portion of the cardiac cycle but have a lower frequency that makes it possible to track them over a longer distance, thus making it a more suitable approach to closed-chest myocardial stiffness estimation.

Recently, studies have been published on the possible relation between increased propagation velocity of naturally occurring MWs and increased myocardial stiffness. Results indicating the possibility of using MW velocity as a parameter for distinguishing between normal and abnormal myocardium have been reported (Santos et al. 2018; Petrescu et al. 2019). A natural next step would therefore be to investigate the possibility of using the propagation velocity of MWs to detect tissue fibrosis. Data on myocardial stiffness and normal propagation velocities of MWs in humans, however, are currently limited.

The propagation of MWs is a short-lived phenomenon. With a typical propagation speed between 1 and 10 m/s (Kanai 2009), the event is over in a matter of milliseconds. Tracking and detecting these waves with ultrasound are made possible only because of the recent developments in high-frame-rate imaging (Tanter and Fink 2014). Instead of transmitting focused beams, diverging waves and plane waves have become popular methods for increasing the frame rate to several thousand frames per second. This is often available in research scanners only, but for this study, data were acquired using weakly focused beams with a clinically available scanner.

To estimate MW propagation velocities, a necessary step is assessment of tissue velocity, often using TDI (Santos et al. 2018; Petrescu et al. 2019). Previous studies have used an anatomical M-mode trace of the tissue acceleration and obtained the MW velocity by calculating the slope of a linear regression line of the maximum of the wave propagation, as seen in Figure 1b. They then assumed that the wave was following the anatomical M-mode. For this study, we

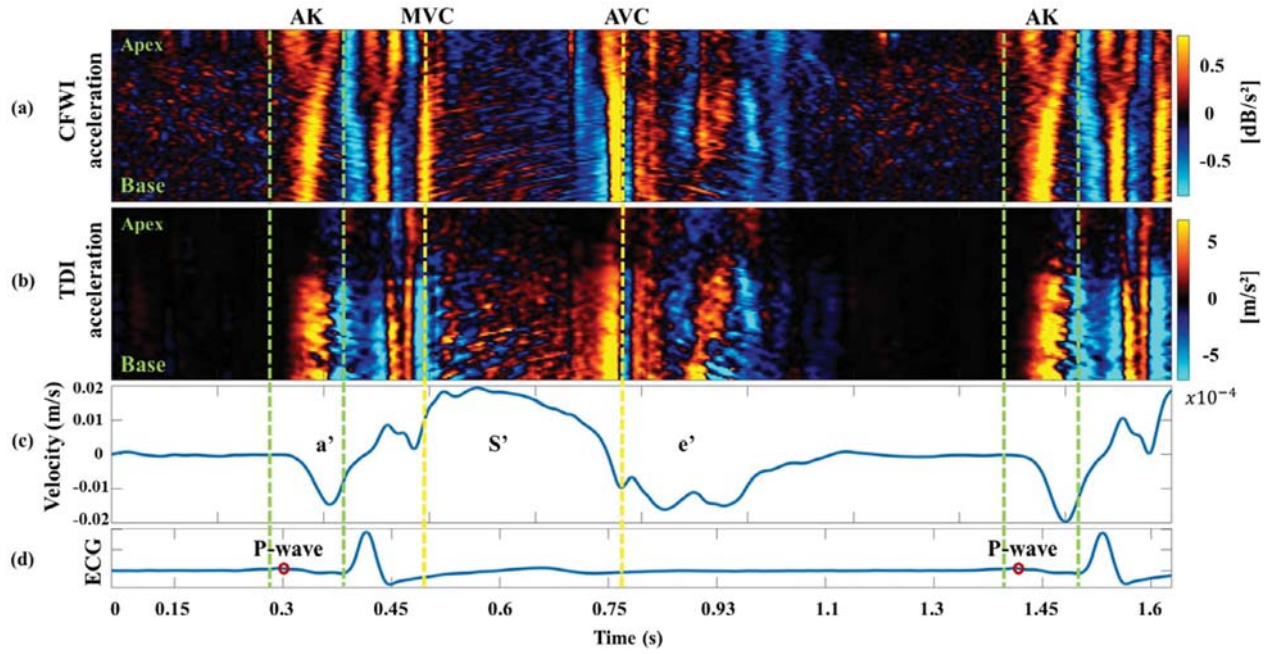

Fig. 1. Mechanical events and waves occurring during the heart cycle for a healthy control participant, here represented by a clutter field wave imaging (CFWI) acceleration M-mode (a), a tissue acceleration M-mode (b), a tissue velocity trace from tissue Doppler imaging (TDI) estimation (c) and the electrocardiogram (ECG) trace (d) for timing purposes. The mechanical waves originating from mitral valve closure (MVC), aortic valve closure (AVC) and the atrial kick (AK) are delimited by *yellow* (MVC and AVC) and *green* (AK) *vertical dotted lines*. The P-wave in the electrocardiogram (ECG) is marked with a *red circle.*

developed and tested a novel approach to estimating the propagation velocity of MWs. The method uses high-frame-rate ultrasound combined with a signal processing method called clutter filter wave imaging (CFWI) (Salles et al. 2019) and a novel 2-D mechanical wave velocity estimation method assuming that the waves take the shorter path between two spatial points. The purpose of CFWI is to filter ultrasound signal data to visualize and detect MWs propagating through myocardial tissue without using a conventional tissue motion estimator. CFWI has been reported to have a better signal-to-noise ratio (SNR) than TDI (Salles et al. 2019) and has previously been used for MW velocity estimation in the carotid artery and the left ventricle (Salles et al. 2019) and for mechanical activation wave detection (Kvale et al. 2019).

Several MWs occur during the cardiac cycle as a result of the different mechanical events of the heart (visible in Fig. 1). This study focuses on investigating the MWs propagating around the time of the P-wave in the electrocardiogram (ECG). The P-wave coincides with the atrial kick (AK), and we therefore refer to the MW of interest as the AK-wave.

The aim of this study was to detect and measure the velocity of the AK-wave in six different walls of the left ventricle separately and to evaluate the stability of the wave through several heart cycles. Furthermore, we investigated the possibility of using CFWI to distinguish between fibrous and healthy tissue by studying changes in MW propagation velocity between healthy controls and patients with pathology, and then correlated our results against MRI data acquired from patients with pathology.

METHODS

High-frame-rate in-phase and quadrature (IQ) data were analyzed with in-house developed software in MATLAB 2017 a (The MathWorks, Natick, MA, USA).

Study population

The study population consisted of a control group of 10 healthy volunteers and 20 patients at least 3 weeks past their first ST-elevation myocardial infarction (MI) (Lervik et al. 2017). The inclusion criteria included age <75 y, peak troponin T >1000 ng/L, estimated glomerular filtration rate >60 mL/min and New York Heart Association functional class <III. Exclusion criteria were previous MI, contraindications to MR contrast/ultrasound contrast, severe heart failure and chronic atrial fibrillation. No patients were excluded because of poor-quality echocardiograms; however, one patient could not complete the late gadolinium enhancement (LGE)-MRI examination because of claustrophobia. Percutaneous coronary intervention was performed in all patients as appropriate during the acute phase, and all patients were examined with acute coronary angiography. The control group was not examined with LGE-MRI. Population characteristics are summarized in Table 1 and outlined in greater detail in Lervik et al. (2017). Informed consent was obtained from all study participants, and the study was approved by the regional ethics committee for medical research ethics and conducted according to the Helsinki Declaration.

Echocardiographic acquisition

High-frame-rate IQ data were acquired from the three apical views (Fig. 2) (two-chamber, four-chamber and apical long-axis), ranging from 1000 to 1200 frames/s. Each acquisition lasted about four heart cycles. A Vivid E9 scanner with a M5 S-D probe (GE Vingmed Ultrasound AS, Horten, Norway) with a center frequency of 2.44 MHz was used. The setup used two wide transmit beams to cover the ventricular walls from the apical view. The transmit beams covered the two 20˚ outermost subsectors of the acquired sector, and the sector width was manually adjusted to cover the LV walls within the two subsectors. The method used 16 receive lines for each wide transmit (Hergum et al. 2007), the lateral resolution was 8.3 mm for a transmit focus of 30 cm, and the beamforming method was a conventional delay-and-sum algorithm. Data from the ventricular cavity were not acquired. The setup is described in detail in Brekke et al. (2014). All echocardiographic data were acquired by experienced sonographers.

MRI

The examinations were performed with a 1.5-T Siemens Avanto (Siemens Medical, Erlangen, Germany) with a six-channel radiofrequency coil. A gadolinium-based contrast agent was administered, and contrast-enhanced images were acquired 10 min later using a

Table 1. Population characteristics

Characteristic	MI patients (n = 20)	Healthy volunteers (n = 10)
Mean age (y)	60 ± 5.9	34 ± 15.2
No. of males	18	10
Days from infarct to US examination	146 (21–356)	-
Days from infarct to LGE-MRI	296 (101–436)	-
Culprit lesion		-
LAD	40%	-
CX	25%	-
RCA	35%	-
Infarct size	12.1 ± 4.9%	-
Left ventricular ejection fraction	56 ± 8%	54 ± 6%

MI = myocardial infarction; LGE-MRI = late gadolinium enhancement magnetic resonance imaging; LAD = left anterior descending coronary artery; CX = circumflex coronary artery; RCA = right coronary artery; US = ultrasound.

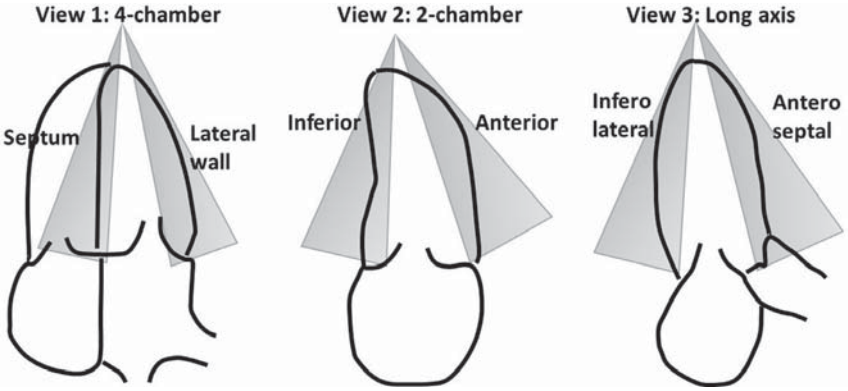

Fig. 2. Three apical views were acquired for each participant: the four-chamber view on the left reveals the septum and the lateral wall; the two-chamber view in the middle reveals the inferior and anterior walls; and the long-axis view on the right reveals the inferolateral and anteroseptal walls. Only the subsectors depicted were imaged, not the blood cavity.

phase-sensitive inversion–recovery balanced steady-state free precession sequence (Lockie et al. 2009). The same apical views were acquired for ultrasound and MRI: four-chamber, two-chamber and long-axis views. The images were acquired during end-expiratory breath hold (10–15 s), in end-diastole, before atrial contraction. MRI was performed for 20 patients. The LGE-MRI is explained in more detail in Lervik et al. (2017).

Clutter filter wave imaging

The principle underlying CFWI is explained in Salles et al. (2019). In blood flow, a clutter filter is generally used to reject all tissue motion from the data. According to the principle underlying CFWI, however, certain tissue velocities are tracked by attenuating them using a high-pass clutter filter on the IQ data. The resulting B-mode image series, after filtering, will display MWs propagating as dark bands (Salles et al. 2019). The propagation velocities of these dark bands can then be tracked to find the propagation velocities of the mechanical waves.

The most important parameter of the filter is the cutoff frequency. The normalized cutoff frequency, *fcn*, of the filter was defined as

$$fc_n = V_c / v_{Nyq} \quad (1)$$

with

$$v_{Nyq} = \frac{c_0 \times \mathrm{FPS}}{4 f_0} \quad (2)$$

and

$$f_c = f_{c_n} \times \mathrm{FPS}/2 \quad (3)$$

where V_c is the cutoff velocity, c_0 is the speed of sound, FPS is the frame rate, f_0 the transmit frequency, v_{Nyq} the Nyquist velocity and f_c the cutoff frequency in hertz.

The first step of the method was to extract high-frame-rate IQ data from the ultrasound scanner (Fig. 3a). In the second step, to suppress tissue velocities of interest, a third-order high-pass filter was applied. A cutoff frequency of 120 Hz, corresponding to a cutoff velocity of about 2.6 cm/s, was used. Further, filtered B-mode images were obtained by envelope detection of the absolute value of the filter output (Fig. 3b). The filtered B-mode images were then differentiated in time (between two successive frames) to obtain the acceleration of the filtered output, here referred to as CFWI acceleration (Fig. 3c). Finally, the SNR was improved by performing temporal smoothing using a third-order low-pass Butter filter with a cutoff frequency of 30 Hz.

The cutoff frequency used for the high-pass filter was found from tissue velocity (using TDI estimation) around the time of a′- and AK-wave propagation. The tissue velocities were converted to cutoff frequency using eqn (1), with V_c as the tissue velocity.

Tissue Doppler imaging

Tissue velocity was estimated using conventional 1-D autocorrelation of the complex IQ data with a temporal lag of 1 in the axial direction (Viola and Walker 2003; Brekke et al. 2014). The estimates were smoothed using a low-pass filter of order 3 and cutoff frequency 30 Hz, as for CFWI for a fair comparison, then with a moving average of size 2×2 samples. Velocity was then obtained using the equation

$$\hat{V} = \frac{\angle R_x(1) \times v_{Nyq}}{\pi} \quad (4)$$

where $\angle \hat{R}_x(1)$ represents the phase angle of the spatio-temporally filtered estimates. Tissue acceleration was estimated as the time derivative of the tissue velocity.

The tissue velocity was used for two things in this study. First, the maximum tissue velocity of the a′-wave

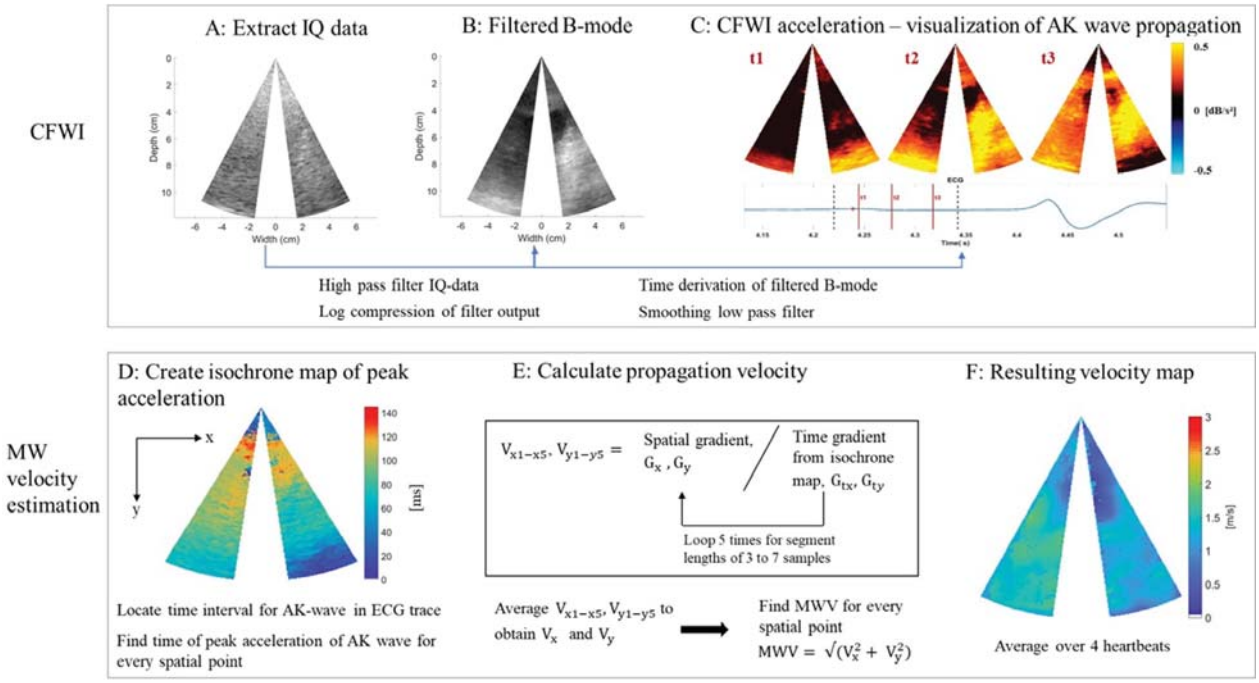

Fig. 3. Flow chart for mechanical wave (MW) velocity estimation. (a) Example of an acquired B-mode image. (B) B-Mode image that has been high-pass filtered and envelope detected. (b−c) Steps of the clutter field wave image (CFWI) acceleration estimation. (c) AK-Wave represented by CFWI acceleration at three different time points after the P-wave on the electrocardiogram (ECG). Propagation of the AK-wave is first observed in the basal lateral wall, then through the lateral wall and the septum toward the apex. (d) Steps involved in creating an isochrone map of the time and location of the maximum acceleration of the AK-wave. (e) Algorithm and equations for calculating the MW velocity. (f) Resulting velocity map obtained from (e) and eqn (5). IQ = in-phase and quadrature.

of the tissue Doppler trace (Fig. 1c) was found for each patient and used for the cutoff frequency value in the CFWI estimation. Second, the tissue acceleration was used for mechanical wave velocity analysis (the tissue acceleration M-mode is illustrated in Fig. 1b).

Mechanical wave velocity estimation

MW propagation velocity was estimated automatically for every spatial point in the acquired data. Figure 3c illustrates the propagation of the AK-wave in the left ventricle represented by CFWI acceleration, and the steps of the velocity estimation are illustrated in Figure 3 (d−f). First, the sample size of the CFWI acceleration image series was converted to a regular grid and interpolated to achieve the same spatial sampling for the axial and lateral directions. Then, the time of the P-wave was automatically localized in the ECG trace to find and define the time interval of AK-wave propagation. Within this interval, a maximum/peak CFWI acceleration was found for every spatial point, resulting in a 2-D isochrone map where the color scale maps to time (ms) to peak acceleration (Fig. 3d). To find the propagation velocity of the AK-wave, velocity was first estimated separately in the two spatial directions x and y (Fig. 3e). This was achieved by calculating gradients from the isochrone map to velocity of propagation. The gradients were calculated in five iterations for segment lengths of three to seven samples (equal to 4.8−11.2 mm), resulting in five velocity matrices in each spatial direction. These were then averaged to obtain one 2-D velocity matrix in each direction, V_x and V_y. Velocities >100 m/s or <0 m/s were excluded from V_x and V_y before they were combined into one vector matrix using the equation

$$\mathrm{MWV} = \sqrt{\left(V_x^2 + V_y^2\right)} \quad (5)$$

where MWV is the MW velocity matrix. A velocity matrix was generated for each of the four heartbeats, for each view, for each subject. The average over the four heartbeats for one view resulted in a velocity map of the left ventricle (Fig. 3f). From this, a resulting average velocity value was calculated for each of the six imaged walls of the left ventricle per subject (Table 2). The entire imaged sectors were used for MW velocity calculation.

Fibrosis detection from LGE-MRI

The myocardial and infarct borders were semi-automatically traced in the MR images. An area with a pixel intensity 1.8 standard deviations (SD) greater than that of the healthy myocardium was considered infarcted.

Table 2. Mechanical wave velocity

Volunteer	MI location LGE-MRI	Septum (m/s)	Lateral (m/s)	Inferior (m/s)	Anterior (m/s)	IF (m/s)	AS (m/s)
1	I, IF	2.3 ± 0.2	1.5 ± 0.2	*2.1 ± 0.1*	2.4 ± 0.2	***2.5 ± 0.1***	1.6 ± 0.2
2	S, I, IF	***2.0 ± 0.1***	2.1 ± 0.1	*1.9 ± 0.1*	2.4 ± 0.3	***2.8 ± 0.0***	1.5 ± 0.1
3	L, IF	1.9 ± 0.1	***2.5 ± 0.1***	1.8 ± 0.1	2.7 ± 0.1	***2.2 ± 0.1***	1.7 ± 0.1
4	-	2.1 ± 0.2	2.4 ± 0.2	2.2 ± 0.1	2.9 ± 0.3	1.8 ± 0.0	2.4 ± 0.1
5	S, L, IF	***2.2 ± 0.1***	***2.2 ± 0.2***	2.2 ± 0.1	2.5 ± 0.1	***1.8 ± 0.9***	1.5 ± 1.0
6	L, I, IF	2.0 ± 0.2	***2.3 ± 0.1***	***2.9 ± 0.2***	2.1 ± 0.3	***2.4 ± 0.1***	1.5 ± 0.1
7	L, A, IF, AS	1.9 ± 0.3	***2.6 ± 0.2***	1.8 ± 0.2	*2.1 ± 0.3*	*1.2 ± 0.7*	*1.5 ± 0.8*
8	L, I, IF	1.6 ± 0.2	*1.9 ± 0.0*	*1.4 ± 0.1*	1.7 ± 0.2	*1.5 ± 0.3*	1.7 ± 0.3
9	S, I, IF	***2.1 ± 0.2***	2.3 ± 0.1	***2.7 ± 0.1***	3.1 ± 0.4	***2.8 ± 0.1***	1.6 ± 0.3
10	L, I, IF	1.5 ± 0.0	*1.7 ± 0.1*	***3.0 ± 0.1***	2.1 ± 0.4	***2.6 ± 0.1***	1.8 ± 0.2
11	S, I, IF	***2.2 ± 0.1***	2.5 ± 0.1	***2.7 ± 0.2***	2.9 ± 0.3	***2.0 ± 0.1***	2.3 ± 0.3
12	L, IF	1.8 ± 0.3	*2.0 ± 0.1*	-	-	***2.4 ± 0.1***	1.6 ± 0.1
13	A	2.1 ± 0.1	3.3 ± 0.3	2.3 ± 0.2	***3.1 ± 0.1***	-	-
14	A	2.3 ± 0.1	1.4 ± 0.1	2.2 ± 0.1	*2.8 ± 0.1*	1.5 ± 0.1	2.7 ± 0.1
15	S, I, IF	***2.5 ± 0.2***	1.7 ± 0.1	*1.6 ± 0.2*	2.1 ± 0.3	*1.7 ± 0.1*	1.7 ± 0.2
16	A, AS	2.0 ± 0.2	1.8 ± 0.2	1.9 ± 0.2	*2.2 ± 0.3*	1.2 ± 0.1	*1.6 ± 0.1*
17	S, L, I, A	***2.3 ± 0.1***	***2.2 ± 0.0***	***2.3 ± 0.1***	***2.9 ± 0.2***	-	-
18	A, AS	2.0 ± 0.2	1.8 ± 0.1	1.9 ± 0.2	*2.2 ± 0.2*	1.4 ± 0.1	*2.4 ± 0.1*
19	S, I, IF	***2.2 ± 0.1***	1.8 ± 0.1	*1.9 ± 0.4*	2.2 ± 0.1	*1.6 ± 0.1*	2.0 ± 0.2
20	S, IF	*1.9 ± 0.1*	2.0 ± 0.1	-	-	***2.1 ± 0.1***	1.4 ± 0.2
Mean	-	2.0 ± 0.2	2.2 ± 0.4	2.1 ± 0.5	2.5 ± 0.5	2.0 ± 0.5	1.8 ± 0.4
Mean Controls	-	1.6 ± 0.4	1.8 ± 0.4	1.8 ± 0.4	2.5 ± 0.4	1.4 ± 0.4	2.4 ± 0.4
p Value		0.02	0.04	0.09	0.5	0.007	0.75
Sensitivity (%)		87.5	62.5	50	33	71.4	0

S = septum; L = lateral wall; I = inferior wall; A = anterior wall; IF = inferolateral wall; AS = anteroseptal wall; - = missing ultrasound data.
*The standard deviations for the patient come from the velocity averaged over four heart cycles.
Velocities in *italic* indicate myocardial infarction found with late gadolinium enhancement magnetic resonance imaging, and velocities in **boldface** and italic indicate matches between myocardial infarction and high mechanical wave velocity.

The results were reported in a 16-segment model (basal, mid- and apical segments of each of the six LV walls), with the infarct size as a percentage of fibrosis of the total segment. The analysis was performed with Segment, Version 1.9.r2959. The method for detecting fibrosis detection from MRI data is described in more detail in Lervik et al. (2017).

Comparison of patients and controls

The MW velocity values obtained from CFWI analysis of the ultrasound data for the 10 controls were averaged for each wall to use as a comparison for the patients (Table 2). The MW velocities of each patient were compared wall by wall against the average MW velocities and SD of the controls. Patients and controls were compared three times, with a different threshold for a positive fibrosis find in the patients for each round. First, the high range of the control velocities was used (average velocity plus standard deviation, eqn [6]), then the average only (eqn [7]) and, last, the low range of the average control velocities (average velocity minus standard deviation, eqn [8]).

$$V_{\text{patient}} > \text{AV}_{\text{controls}} + \text{SD}_{\text{controls}} \quad (6)$$

$$V_{\text{patient}} > \text{AV}_{\text{controls}} \quad (7)$$

$$V_{\text{patient}} > \text{AV}_{\text{controls}} - \text{SD}_{\text{controls}} \quad (8)$$

Thus, all patient velocities above the threshold of the control velocities were defined as a positive fibrosis find. The findings from the CFWI data were then compared with the MRI results to find corresponding segments of fibrosis.

Statistical analysis

The normality of the data was validated using the Shapiro–Wilk test. A two-tailed Student *t*-test assuming unequal variances (Welch) was performed to compare the MW velocities of the healthy volunteers against the MW velocities of the patients. A two-sided p value of 0.05 was considered to indicate statistical significance.

RESULTS

CFWI was used to estimate the MW velocity for six walls of the left ventricle for 30 subjects. The velocities were used to define healthy and fibrous tissue, and the results were compared with fibrosis finds from LGE-MRI.

Clutter filter wave imaging

Table 2 summarizes the MW velocities of the patients and the average MW velocities of the controls for each of the six imaged LV walls. The table indicates that for 4 of 20

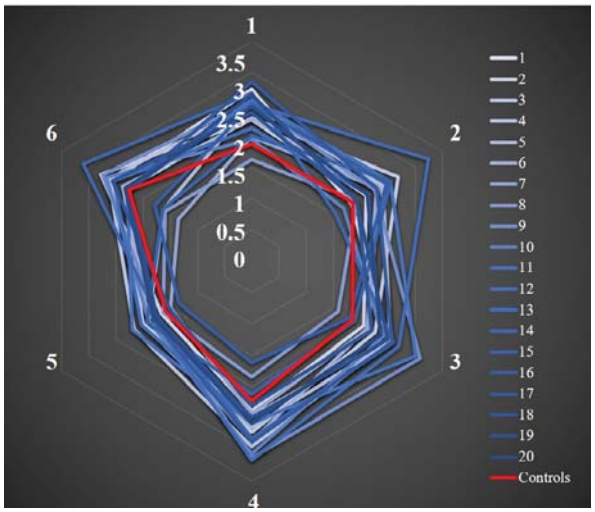

Fig. 4. Area plot of the mechanical wave velocities for each patient and the average of the controls. Each of the six walls is represented by an angle/point of the hexagon. The average of the controls is indicated by the red line.

patients, ultrasound data were missing for one view. These values are also visualized in Figure 4, which illustrates the MW velocities as areas in a radar plot. The average of the controls is outlined in red. Each point/angle of the hexagons represents an LV wall, and the vertical axis is the MW velocity in meters per second. The average of the controls occupied a smaller area than did most of the patients. In Figure 5 are velocity maps obtained for a healthy control (a) and a patient (b) with detected infarcts in the septum, inferior and inferolateral walls. Lower velocities could be observed for all views for the control compared with the patient. Furthermore, a statistically significant difference was found when all velocities for the two groups were compared (p value = 0.003). When the two groups were compared wall by wall, a statistically significant difference (p value <0.05) was found for three of six walls (Table 2). No statistically significant difference was found for the inferior, anterior and the anteroseptal walls.

TDI comparison

In Figure 1b is an anatomical color M-mode for tissue acceleration for a healthy control subject. An attempt was made to estimate MW velocity using TDI acceleration as a comparison for CFWI acceleration, but for this specific application and for the AK-wave, the results from TDI estimation were found to have insufficient data quality in 70.1% of the data acquisitions. The data quality was assessed by visual inspection of anatomical M-mode traces, and poor quality was defined by the inability to distinguish the propagation of the MW from noise. Therefore, the decision was made not to continue with the production of MW velocity results using this method for this data set. The difference in data quality and SNR is observable in Figure 1, where M-modes from CFWI acceleration (a) and TDI acceleration (b) for the same wall are plotted. The AK-wave is marked in the plots with *vertical dotted green lines*, and it can be observed that in the basal parts of the wall, both methods have a good SNR, but in the apical regions, in particular, TDI acceleration, with the implementation used for this study, failed compared with CFWI acceleration.

MRI fibrosis findings

Table 3 summarizes the findings from the MRI data. MRI was performed on 19 patients. One patient was excluded because of claustrophobia. For a simpler

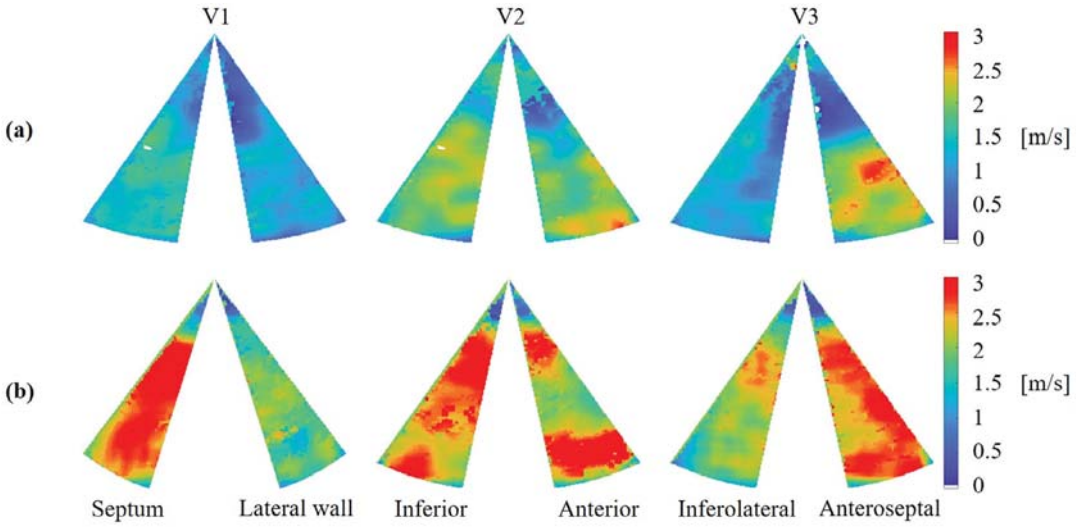

Fig. 5. Example velocity maps obtained from a healthy control (a) and a patient (b) with detected infarcts in the septum, inferior and inferolateral walls. The views and walls are the same as in Figure 2. (a) Homogenous low-velocity maps for the control. (b) Higher velocities can be observed in most walls for this patient.

Table 3. Magnetic resonance imaging results

No. of walls	No. of walls >10%	No. of detectable infarcts >10%	No. of infarcts >60%	No. of infarcts >75%
114	54	49	21	12

Table 4. Comparison of clutter filter wave imaging and magnetic resonance imaging results*

Threshold	Sensitivity			FPs >10%	Missed			Specificity		
	>10%	>60%	>75%		>10%	>60%	>75%	>10%	>60%	>75%
High†	59.2‡	61.9	66.7	13.2	40.8	38.1	33.3	74.6	65.9	63.9
Mean	82.0	85.7	83.3	20.2	18.0	14.3	16.7	58.9	45.1	44.1
Low	90.0	90.5	91.7	37.7	10.0	9.5	8.3	22.1	17.9	17.2

FPs = false positives.
* In the first column are the thresholds used in the comparison of control and patient mechanical wave velocity values to define a positive fibrosis find.
† High = mean + standard deviation (eqn [6]). Mean (Eq. [7]). Low = mean − standard deviation (eqn [8]).
‡ All values are percentages.

comparison with the ultrasound data, the 16-segment model was converted into a six-wall model, and the segment from the MRI with the highest percentage of fibrosis was used as the value representing a wall.

The table indicates the total number of walls acquired by MRI, the total number of infarcts found from MRI analysis, and the total number of infarcts that could be detected in the ultrasound data because of missing ultrasound data for 8 of 120 walls (Table 2). The infarcts were divided into three groups based on the percentage of fibrosis found in a segment. The sizes of these infarcts varied from >10%, to >60%, to >75% of the imaged LV wall, and the number of infarcts of these sizes found is provided in Table 3. The locations of the infarcts for each patient are given in Table 2 (column 2 and velocities in *italic*).

CFWI and MRI fibrosis comparison

Table 4 summarizes the findings from the comparison of CFWI with MRI fibrosis results. The table indicates the sensitivity in the three groups of infarct sizes, for the three definitions used to define a positive fibrosis find in the CFWI data. The table also lists the percentage of false-positive detections for infarcts with a size >10%, where the CFWI method found a high MW velocity but no fibrosis was detected in the MRI data. Furthermore, the table gives the percentages of infarcts missed by the CFWI method, where a normal MW velocity was estimated but LGE-MRI found fibrosis. Finally, specificity gives the probability of correctly detecting non-fibrous walls. Increasing sensitivity was observed for the lower thresholds in the CFWI fibrosis detection method. Further, the number of false positives increased, while the number of missed infarcts decreased.

For the most conservative threshold (eqn [6]), the sensitivity and specificity for infarcts remained close to or >60%. The sensitivity was observed to increase with increasing infarct size, while specificity decreased with increasing infarct size. The rate of detection of false positives was 13.2%. Table 2 lists the locations of the infarcts (in italic), the locations where fibrosis was detected by both methods (bold and italic) and the sensitivity for each wall.

The authors were not blinded to the LGE-MRI results during processing of the MW velocities, as we attempted to find the best parameters to differentiate both groups, but the medical doctor performing the ultrasound acquisition was blinded to the MRI results.

Feasibility and reproducibility

The main parameter in the CFWI MW velocity estimation method is the cutoff frequency used for the high-pass clutter filter. The sensitivity of this parameter was tested and is displayed in Figure 6a, with the y-axis as the deviation (in m/s) from the MW velocity results from the value that was used for this study (normalized cutoff velocity of 0.2), for each of the 30 persons. A lower normalized cutoff frequency gave lower MW velocities for all but 1 of 30 persons, while increasing the normalized cutoff frequency yielded higher MW velocities for all but 3 of 30 persons. The average deviation is displayed in the figure in *yellow* and ranges from −0.3 m/s for a normalized cutoff frequency of 0.1 to 0.1 m/s for a normalized cutoff frequency of 0.3. The maximum deviation was found to be 0.7 m/s for one patient, but only for 6.7% of the estimations was a deviation larger than ±0.35 m/s found.

The MW velocities for each wall were the result of averaging over 4 heartbeats. The stability and reproducibility of the AK-wave over several heart cycles is

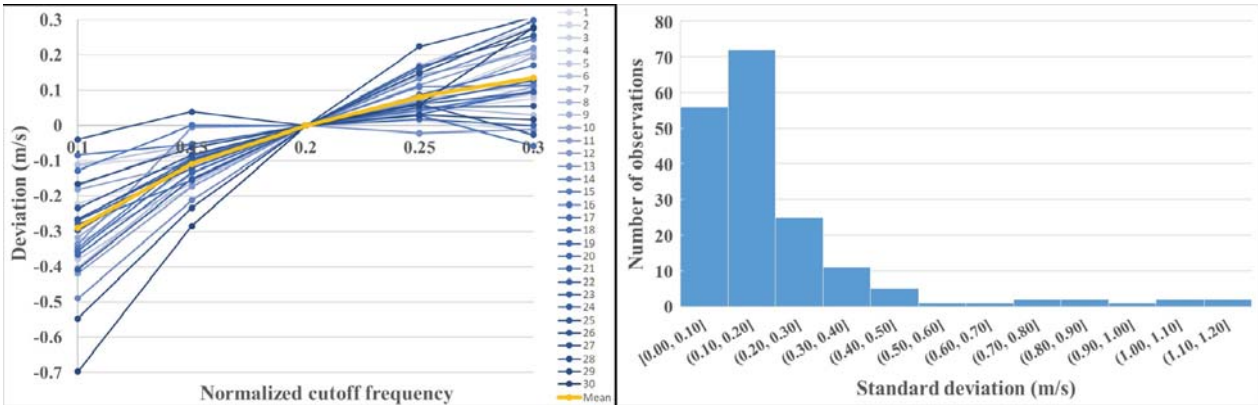

Fig. 6. Sensitivity analysis of the mechanical wave (MW) velocity estimation method. (a) the Effect on MW velocities of changing the cutoff frequency of the clutter field wave imaging high-pass filter. The average for all 30 patients is in *yellow*. (b) Standard deviations obtained from averaging the MW velocities found over four heart cycles. In total there were 180 observations, one for each wall of each of the 30 patients.

reflected by the standard deviations, which ranged from 0.02−1.3 m/s. Figure 6b is a histogram plot of the SD obtained from all 30 persons, with the number of observations on the y-axis. One hundred forty of 172 observations (82.0%) had a standard deviation <0.3 m/s.

Additionally, an analysis of the effect of changing the cutoff frequency on sensitivity and specificity of the method (for infarcts >10% in size) was performed, and the result is illustrated in Table 5. The sensitivity was highest for a normalized cutoff frequency of 0.2, used for the analysis in this study, and lowest for 0.3 at 53.1%. Furthermore, the specificity was the lowest for the same cutoff frequency at 77.2% and the highest for 0.15 and 0.25 at 84.1%, compared with 80.7% for 0.2.

Table 5. Stability of sensitivity and specificity

NCF	Sensitivity	Specificity
0.1	59.2	82.5
0.15	55.1	84.1
0.2	59.2	80.7
0.25	55.1	84.1
0.3	53.1	77.2

NCF = normalized cutoff frequency.

DISCUSSION

In this feasibility study we developed and tested a novel method for estimating MW velocity in the left ventricle for the purpose of detecting fibrosis in the human myocardium using CFWI. The MW velocity values were evaluated by comparison between patients and healthy controls, and against fibrosis findings from the non-invasive gold standard LGE-MRI. The data were obtained from an affiliated group and have previously been used for a study with a similar objective (Lervik et al. 2017); however, the ultrasound processing method developed in this study represents a different approach to detection of myocardial infarctions.

The MW velocities obtained using CFWI analysis are listed in Table 2, and the patients and controls are compared in Figures 4 and 5. In Figure 4 the velocities per wall are displayed in an area plot revealing that the area of the controls was smaller than that of most of the patients, while in Figure 5, velocity maps obtained from a control (a) were found to have a more homogenous velocity distribution, in addition to lower velocities overall, compared with velocity maps obtained from the patient (b). For three of the imaged walls (inferior, anterior and anteroseptal), no statistically significant difference in MW velocity was found between the patient and control groups (Table 2). A possible explanation for the anterior and anteroseptal walls is that they accounted for only 18% of the detected infarcts, and therefore, a higher similarity in the velocities of the two groups would be expected. Twenty percent of the infarcts were located in the inferior wall; thus, this explanation does not apply. However, these results seem to be related to the difference in sensitivity between ultrasound and LGE-MRI per wall (Table 2), as it is lower for these walls (50%, 33% and 0%, respectively) compared with the septum, lateral and inferolateral walls (87.5%, 62.5% and 71.4%, respectively). An explanation for the poor detection rate in the anterior and anteroseptal walls could be related to the equal or higher average velocities found in controls compared with patients (2.5 ± 0.4 m/s vs. 2.5 ± 0.5 m/s and 2.4 ± 0.4 m/s vs. 1.8 ± 0.4 m/s, respectively). The method for fibrosis detection is based on the average velocity of the controls (eqn [6]), which can be limiting. Overall, a sensitivity and specificity near or >60% was obtained for all investigated infarct sizes, with a false-positive detection rate of only 13.2% (Table 4). Thus,

these results were encouraging in confirming the hypothesis that increased AK-wave velocity could be used as an indicator for fibrosis, although only for the septal, lateral and inferolateral walls of the LV. The reason for the higher velocities of the anterior and anteroseptal walls in the control group was not studied for this project. Several published studies on natural MWs have considered one or two LV walls only (Santos et al. 2018; Petrescu et al. 2019). Our result could indicate that this might be insufficient as we currently do not know how one fibrous region affects neighboring or other regions of the left ventricle. Therefore, it is possible that the MW velocities should be evaluated for the whole left ventricle using 3-D data and not only wall by wall.

A comparison of CFWI and TDI was attempted in this study as TDI is the most often used method for tissue motion estimation. For this data set and for the AK-wave, the TDI method failed to give results that were considered adequate for MW velocity estimation. An example is illustrated in Figure 1b, where the signal was lost toward the apex. CFWI has previously been reported to have a better SNR than TDI for MW velocity estimation, especially in the apical region (Salles et al. 2019), mainly because the clutter filter removes the clutter noise in the near field of the ultrasound beam.

Three different thresholds were used to define a positive fibrosis find in the ultrasound data (eqns [6], [7] and [8]). As expected, lowering the threshold for a positive fibrosis find increased the sensitivity and the false-positive rate (Table 4). For all thresholds, the sensitivity remained fairly stable for increasing infarct size, while the specificity decreased, which means that more healthy subjects would be identified as pathologic for larger infarcts. This was caused by the increasing number of false positives that resulted from the ultrasound method's the current inability of the ultrasound method to separate infarct sizes. For comparison, the threshold analysis to find fibrosis was also performed for the controls. For the high-range threshold, 15.4% of the walls of the controls were found to have a high velocity, indicating stiffer tissue. Of these, 75% belonged to one control, and the remaining 25% to another. For the mid-range threshold, the average, 51.9% of the walls were found to have higher velocities, as expected, while for the low-range threshold, 73% of the walls were found to be fibrous. From this we could conclude that the mid- and low-range thresholds were untrustworthy definitions for a positive fibrosis find, as the sensitivity in the controls exceeded 50%.

The sensitivity of the most important parameter of the developed method is examined in Figure 6a, which illustrates the effect on MW velocities of changing the normalized cutoff- frequency of the CFWI filter. For a very few outliers, changing this parameter had a fairly large effect, changing the velocity up to 0.7 m/s, but most observations (93.3%) revealed a small deviation from the results obtained with the chosen cutoff frequency of less than 0.35 m/s. This indicates that the method had a low sensitivity to changing the cutoff frequency. Additionally, the stability of the sensitivity and specificity values (in Table 4) was tested for changing cutoff frequencies for infarcts $>10\%$ in size (Table 5). The sensitivity decreased from 59.2% to 53%, and the specificity, from 80.2% to 77%. This result indicates that while the method produced fairly stable MW velocities for different cutoff frequencies, it did have an effect on sensitivity and specificity. A limitation of the developed method is therefore that a constant cutoff frequency was used for all walls and all subjects. The method could possibly be improved by applying an adaptive cutoff frequency specific to the tissue velocity of participant and LV wall. The stability of the MW velocities over several heart cycles was evaluated in Figure 6b, which illustrates that 82.0% of the velocity estimates had a small standard deviation <0.3 m/s. This result indicates that the propagation of the AK-wave was stable over time and could therefore be considered a trustworthy mechanical event in the heart cycle to be used for analysis.

Comparison of the CFWI results against MRI fibrosis findings yielded fairly good sensitivity. Nonetheless, several of the larger infarcts were missed, and several false infarcts were detected by CFWI (Table 4). Several possible sources of error likely caused these discrepancies, such as data acquisition and image quality. There is a trade-off between spatial resolution and frame rate for ultrasound imaging. Higher frame rate resulted in a loss of spatial resolution that inevitably made the image quality poorer and, thereby, the data acquisition more difficult, as obtaining the correct views and keeping the LV walls within the sectors became more challenging. Additionally, with the acquisition method used, the mid-part of the apex was not depicted and thus not considered for the MW velocity estimation (Fig. 2). At the time of data collection, imaging two sectors only was an acquisition method developed to achieve high frame rate. This limitation can be overcome by using plane and diverging wave imaging techniques (Tanter and Fink 2014). Furthermore, confirming that the views from ultrasound and MRI were aligned was difficult without microcrystals implanted in the myocardium. Therefore, ensuring that the exact same tissue was imaged was not possible. Moreover, the two modalities were aiming at detecting tissue stiffness in different stages. LGE-MRI is the gold standard for detecting myocardial fibrosis (Iles et al. 2008), while with CFWI we aimed to detect tissue stiffness through MW velocities. Although fibrotic tissue is stiffer than healthy tissue, it is not the only cause of increased stiffness. Stiffer tissue has, for example, been

reported to be age related (Villemain et al. 2019). Additionally, tissue can become stiffer at early stages of ischemia before fibrosis develops (Amano et al. 1987; Ventura-Clapier and Veksler 1994). This serves as a possible explanation for the false positives detected.

For this study, we have referred to the AK-wave as a naturally occurring mechanical wave without specifying more about its nature. This wave was chosen because it might be easier to detect diseases when the myocardium is in a relaxed state (Pislaru et al. 2004); additionally, it had a very strong signal. The wave has been reported to propagate through the left ventricle from the base toward the apex along the myocardial fibers, with a propagation speed of 1 to 4 m/s (Kanai 2009). Thus, a change in the fibers, such as different orientation, stretching and increased stiffness, was expected to cause a change in the propagation velocity. Figure 1 illustrates the timing of the AK-wave, during the a′-wave in the TDI velocity trace (c) and slightly after the P-wave in the ECG (d), corresponding in time to the atrial kick. Thus, it has been speculated that the origin of this wave is the mechanical force of the AK (Kanai 2009) and that it is a shear wave (Engel 2017). However, the trigger for and the nature of this wave remain unknown. Several MWs occur during the cardiac cycle as a result of mechanical events, and studies focused on the waves occurring after mitral and aortic valve closure, in animals (Vos et al. 2017) and humans (Santos et al. 2018; Petrescu et al. 2019), have been reported in the literature. These waves have been described as shear waves, although a pressure wave could also be generated by these mechanical stimuli. This assumption would have an impact on how the results are interpreted. A shear wave would be expected to propagate faster in stiff tissue than in softer, healthy tissue. For a pressure wave, however, the geometry of the medium would have to be considered to recover the mechanical properties of the tissue, indeed according to the Moens−Korteweg equation

$$\mathrm{PWV} = \sqrt{\frac{\mathrm{E_{inc}} * h}{2\, r\rho}} \tag{9}$$

where PWV is the pulse wave velocity, E_{inc} the elastic modulus of the wall, h the wall thickness and ρ the blood density. The equation says that a pressure wave would propagate faster in a smaller left ventricle. Further investigation of this issue was not performed for this study.

A limitation of the developed method is that entire imaged sectors were used for MW velocity calculation, which means that small parts of the sectors could have contained a ventricular cavity instead of tissue. Another limitation of the study is that we are imaging a 3-D phenomenon using 2-D planes. The mechanical wave propagates in three dimensions and could therefore easily propagate in and out of the imaged 2-D planes. We have attempted to mitigate this limitation by using several 2-D planes, but we still do not get the whole picture of the propagation pattern of this wave. CFWI has already been developed for 3-D images and it would therefore be possible to expand this method to three dimensions for future work. A 3-D setup would also be useful in eliminating a limitation of ultrasound imaging, which is the difficulty of imaging the same imaging plane after removing and repositioning the probe. The sensitivity of this variability has not been investigated for this method in this study but should be part of future work with another population study. Additionally, we would like to expand this study to investigate other mechanical events such as the MWs originating from mitral and aortic valve closure to compare our findings for the AK-wave. That could possibly help further our understanding of the local differences in MW propagation velocities for the AK-wave and local tissue stiffness observed in the left ventricle. Unfortunately, the quality of the data for this study was not sufficient to estimate the velocities of the other waves.

CONCLUSIONS

This feasibility study found that high-frame-rate ultrasound data processed with CFWI could be a valuable tool for myocardial fibrosis detection or tissue characterization. We found that with the new method, we were able to detect differences in the MW velocities of healthy controls and infarct patients, and we could detect 60% or more of the infarcts found using LGE-MRI. We have also illustrated that the AK-wave is stable through several heart cycles and is therefore a trustworthy mechanical event to study. These results encourage further investigation. However, there were several missed infarcts and false-positive detections using our method, which could result from poor image quality in the data and from other underlying physiological reasons. This issue needs to be investigated further. Additionally, further testing and validation are required for increasing our knowledge of the physical phenomenon we are observing. The ability of the method developed here to detect myocardial fibrosis remains to be observed in further clinical studies.

Acknowledgments—This work was supported by the Center for Cardiological Innovation (CCI) and the Centre for Innovative Ultrasound Solutions (CIUS), both centers for Research-Based Innovation, supported by the Research Council of Norway.

Conflict of interest disclosure—The authors declare they have no conflicts of interest.

SUPPLEMENTARY MATERIALS

Supplementary material associated with this article can be found in the online version at doi:10.1016/j.ultrasmedbio.2020.04.022.

REFERENCES

Amano J, Jr Thomas J, Lavallee M, Mirsky I, Glover D, Manders W, Randall W, Vatner S. Effects of myocardial ischemia on regional function and stiffness in conscious dogs. Am J Physiol Heart Circ Physiol 1987;252:H110–H117.

Brekke B, Nilsen LC, Lund J, Torp H, Bjastad T, Amundsen BH, Stoylen A, Aase SA. Ultra-high frame rate tissue Doppler imaging. Ultrasound Med Biol 2014;40:222–231.

Dalen H, Thorstensen A, Aase SA, Ingul CB, Torp H, Vatten LJ, Stoylen A. Segmental and global longitudinal strain and strain rate based on echocardiography of 1266 healthy individuals: The HUNT study in Norway. Eur J Echocardiogr 2009;11:176–183.

Engel AJ. Development of cardiac atrial kick shear wave elastography to assess myocardial stiffness. Lincoln: Dissertation, University of Nebraska; 2017.

Ferraioli G, Parekh P, Levitov AB, Filice C. Shear wave elastography for evaluation of liver fibrosis. J Ultrasound Med 2014;33:197–203.

Heimdal A, Støylen A, Torp H, Skjærpe T. Real-time strain rate imaging of the left ventricle by ultrasound. J Am Soc Echocardiogr 1998;11:1013–1019.

Hergum T, Bjastad T, Kristoffersen K, Torp H. Parallel beamforming using synthetic transmit beams. IEEE Trans Ultrason Ferroelectr Freq Control 2007;54:271–280.

Iles L, Pfluger H, Phrommintikul A, Cherayath J, Aksit P, Gupta SN, Kaye DM, Taylor AJ. Evaluation of diffuse myocardial fibrosis in heart failure with cardiac magnetic resonance contrast-enhanced T1 mapping. J Am Coll Cardiol 2008;52:1574–1580.

Kanai H, Satoh H, Hirose K, Chubachi N. A new method for measuring small local vibrations in the heart using ultrasond. IEEE Trans Biomed Eng 1993;40:1233–1242.

Kanai H. Propagation of vibration caused by electrical excitation in the normal human heart. Ultrasound Med Biol 2009;35:936–948.

Kass DA, Bronzwaer JG, Paulus WJ. What mechanisms underlie diastolic dysfunction in heart failure?. Circ Res 2004;94:1533–1542.

Kvale K, Bersvendsen J, Remme E, Salles S, Aalen J, Brekke P, Edvardsen T, Samset E. Detection of regional mechanical activation of the left ventricular myocardium using high frame rate ultrasound imaging. IEEE Trans Med Imaging 2019;38:2665–2675.

Lervik LCN, Brekke B, Aase SA, Lønnebakken MT, Stensvåg D, Amundsen BH, Torp H, Støylen A. Myocardial strain rate by anatomic Doppler spectrum: First clinical experience using retrospective spectral tissue Doppler from ultra-high frame rate imaging. Ultrasound Med Biol 2017;43:1919–1929.

Lockie T, Nagel E, Redwood S, Plein S. Use of cardiovascular magnetic resonance imaging in acute coronary syndromes. Circulation 2009;119:1671–1681.

Nathan M, Ying LC, Pierre C, David B, João L. Assessment of myocardial fibrosis with cardiac magnetic resonance. J Am Coll Cardiol 2011;57:891.

Pernot M, Fujikura K, Fung-Kee-Fung SD, Konofagou EE. ECG-gated, mechanical and electromechanical wave imaging of cardiovascular tissues in vivo. Ultrasound Med Biol 2007;33:1075–1085.

Pernot M, Couade M, Mateo P, Crozatier B, Fischmeister R, Tanter M. Real-time assessment of myocardial contractility using shear wave imaging. J Am Coll Cardiol 2011;58:65–72.

Pernot M, Lee WN, Bel A, Mateo P, Couade M, Tanter M, Crozatier B, Messas E. Shear wave imaging of passive diastolic myocardial stiffness: Stunned versus infarcted myocardium. JACC Cardiovasc Imaging 2016;9:1023–1030.

Petrescu A, Santos P, Orlowska M, Pedrosa J, Bézy S, Chakraborty B, Cvijic M, Dobrovie M, Delforge M, D'hooge J, Voigt JU. Velocities of naturally occurring myocardial shear waves increase with age and in cardiac amyloidosis. JACC Cardiovasc Imaging 2019;12:2389–2398.

Pislaru C, Bruce CJ, Anagnostopoulos PC, Allen JL, Seward JB, Pellikka PA, Ritman EL, Greenleaf JF. Ultrasound strain imaging of altered myocardial stiffness: Stunned versus infarcted reperfused myocardium. Circulation 2004;109:2905–2910.

Prior DL, Somaratne JB, Jenkins AJ, Yii M, Newcomb AE, Schalkwijk CG, Black MJ, Kelly DJ, Campbell DJ. Calibrated integrated backscatter and myocardial fibrosis in patients undergoing cardiac surgery. Open Heart 2015;2 e000278.

Salles S, Løstakken L, Aase SA, Bjåstad TG, Torp H. Clutter filter wave imaging. IEEE Trans Ultrason Ferroelectr Freq Control 2019;66:1444–1452.

Santos P, Samset E, D'hooge J. Volumetric imaging of fast mechanical waves in the heart using a clinical ultrasound system. 2017 IEEE Int Ultrason Symp (IUS), Washington, DC, 2017:1−5.

Santos P, Petrescu A, Pedrosa J, Orlowska M, Komini V, Voigt JU, D'hooge J. Natural shear wave imaging in the human heart: Normal values, feasibility and reproducibility. IEEE Trans Ultrason Ferroelectr Freq Control 2018;66:442–452.

Sutherland GR, Di Salvo G, Claus P, D'hooge J, Bijnens B. Strain and strain rate imaging: A new clinical approach to quantifying regional myocardial function. J Am Soc Echocardiogr 2004;17:788–802.

Tanter M, Fink M. Ultrafast imaging in biomedical ultrasound. IEEE Trans Ultrason Ferroelectr Freq Control 2014;61:102–119.

Urban MW, Pislaru C, Nenadic IZ, Kinnick RR, Greenleaf JF. Measurement of viscoelastic properties of in vivo swine myocardium using lamb wave dispersion ultrasound vibrometry (LDUV). IEEE Trans Med imaging 2013;32:247–261.

Ventura-Clapier R, Veksler V. Myocardial ischemic contracture: Metabolites affect rigor tension development and stiffness. Circ Res 1994;74:920–929.

Villemain O, Correia M, Mousseaux E, Baranger J, Zarka S, Podetti I, Soulat G, Damy T, Hagège A, Tanter M, Pernot M, Messas E. Myocardial stiffness evaluation using noninvasive shear wave imaging in healthy and hypertrophic cardiomyopathic adults. JACC Cardiovasc Imaging 2019;12:1135–1145.

Viola F, Walker WF. A comparison of the performance of time-delay estimators in medical ultrasound. IEEE Trans Ultrason Ferroelectr Freq Control 2003;50:392–401.

Vos HJ, van Dalen BM, Heinonen I, Bosch JG, Sorop O, Duncker DJ, van der Steen AF, de Jong N. Cardiac shear wave velocity detection in the porcine heart. Ultrasound Med Biol 2017;43:753–764.